Thermodynamics, Electrode Kinetics, and Mechanistic Nuances Associated with the Voltammetric Reduction of Dissolved [n -Bu 4 N] 4 [PW 11 O 39 Sn(C 6 H 4)C≡C(C 6 H 4)(N 3 C 4 H 10)] and a Surface-Confined Diazonium Derivative

Md Anisur Rahman, Anisur Rahman, Maxime Laurans, Guillaume Izzet,
Anna Proust, Alan Bond, Jie Zhang

Thermodynamics, electrode kinetics and mechanistic nuances associated with the voltammetric reduction of dissolved [n-Bu$_4$N]$_4$[PW$_{11}$O$_{39}${Sn(C$_6$H$_4$)C≡C(C$_6$H$_4$)(N$_3$C$_4$H$_{10}$)}] and a surface confined diazonium derivative

Md Anisur Rahman[a], Si-Xuan Guo[a, b], Maxime Laurans[c], Guillaume Izzet[c], Anna Proust[c] *,

Alan M. Bond[a, b] * and Jie Zhang[a, b] *

[a] School of Chemistry, Monash University, Clayton, Victoria 3800, Australia

[b] ARC Centre of Excellence for Electrochemical Science, Monash University, Clayton, Victoria 3800, Australia

[c] Sorbonne Université, CNRS, Institut Parisien de Chimie Moléculaire, IPCM, 4 Place Jussieu, F-75005 Paris, France.

Abstract

The power of Fourier transformed large amplitude alternating current voltammetry (FTACV) has been applied to parameterise the reduction of the phospho-tungstate $[PW_{11}O_{39}\{Sn(C_6H_4)C\equiv C(C_6H_4)(N_3C_4H_{10})\}]^{4-}$ polyoxometalate ($K^W_{Sn}[N_3C_4H_{10}]^{4-/5-/6-}$ processes) at glassy carbon (GC), gold (Au) and platinum (Pt) electrodes as well as its GC surface confined $K^W_{Sn}[-]^{4-}$-grafted diazonium derivative in acetonitrile (0.10 M $[n\text{-Bu}_4N][PF_6$. The thermodynamics (E^0) and heterogeneous electron-transfer kinetics (k^0 and α) were estimated using the Butler-Volmer relationship. FTACV provides access to significantly more detailed mechanistic information related to non-conformance to the theory than widely used DC voltammetric methods, especially with the more intricate surface confined electrochemistry. Parameterisation, the level of agreement and systematic variations between experimental and simulated data were established by both an experimenter controlled heuristic method and by a computationally efficient data optimization approach that employed parameter space searches restricted in scope by knowledge of the heuristically based estimations. The first electron transfer process for both acetonitrile soluble $K^W_{Sn}[N_3C_4H_{10}]^{4-}$ and surface confined $K^W_{Sn}[-]^{4-}$ is always significantly faster than the second. The electrode dependence order is $k^0_{GC} > k^0_{Au} > k^0_{Pt}$ for the $K^W_{Sn}[N_3C_4H_{10}]^{4-/5-}$ process. The relatively slower electrode kinetics found for reduction of $K^W_{Sn}[N_3C_4H_{10}]^{4-}$ as compared to some other monomeric Keggin POMs may be due to the long organic chain hindering the approach of the POM to the electrode surface, although differences in ion-paring and other factors also may play a role. Subtle, but systematic differences identified in comparisons of experimental and simulated voltammetry give rise to apparently data analysis method dependent parameterisation and are discussed in terms of nuances not accommodated in the modelling. In the solution phase voltammetry, data obtained by electrochemical quartz crystal microbalance and other techniques are consistent with sold adhering to and modifying the electrode surface following reduction of $K^W_{Sn}[N_3C_4H_{10}]^{4-}$ to $K^W_{Sn}[N_3C_4H_{10}]^{5-}$. Kinetic and thermodynamic dispersion present in the heterogeneous $K^W_{Sn}[-]^{4-}$-grafted electrode are probable causes of non-ideality detected in the surface confined voltammetry of this material. Thus FTACV gives valuable insights into what is needed to provide a more realistic

description of the polyoxometalate/electrode interface in polyoxometalate electrochemistry by revealing subtle nuances that are often overlooked.
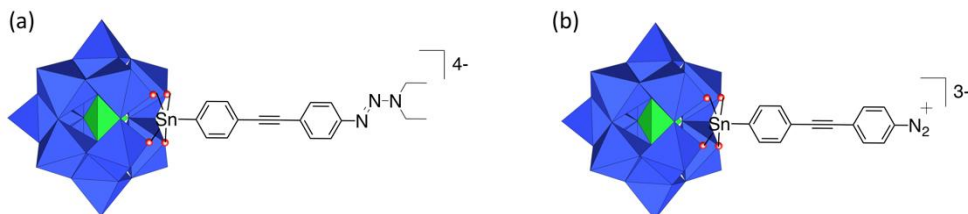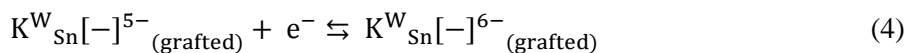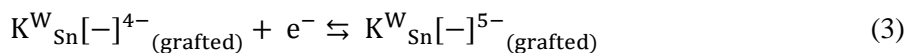
1. Introduction

Nano-sized metal oxoanions, known as polyoxometalates (POMs), are an important class of inorganic clusters that are usually constructed from early transition metals. Their ability to undergo an extensive series of electron transfer reactions when dissolved in solution or attached to electrode surfaces [1-4] has made these anions valuable in applications of electrochemistry in diverse fields such as electrocatalysis [5-7], electrosynthesis [8], biosensing [9, 10] and energy storage [11, 12]. Glassy carbon (GC) has been available as an electrode material [2, 13-15] for over half a century. Much of the recent solution phase and surface confined POM electrochemistry has been reported at this electrode surface to improve selectivity in electroanalysis or to overcome slow electron-transfer kinetics found with use of conventional metal electrodes [16, 17]. The main techniques for electrode modification are largely based on electrostatic [18-20] or covalent attachment [2, 3, 21, 22].

The electrode kinetics of POMs with Keggin and Dawson structures have been reported in studies in solution phase [23-25] and with spontaneously adsorbed forms [26-28]. Relevant to this study, functionalization of POMs has recently been introduced to provide a reactive terminal diazonium group that facilitates surface anchoring to the electrode [2, 3, 22, 29]. In the present study, the thermodynamics (reversible formal potentials, E^0 values) and electrode kinetics (heterogeneous charge transfer rate constant k^0 at E^0 and charge transfer coefficient, α values) of the solution soluble Keggin POM functionalized with a protected diazonium, [n-Bu$_4$N]$_4$[PW$_{11}$O$_{39}${Sn(C$_6$H$_4$)C≡C(C$_6$H$_4$)(N$_3$C$_4$H$_{10}$)}] ([n-Bu$_4$N]$_4$K^W$_{Sn}$[N$_3$C$_4$H$_{10}$], Figure 1 (a)) is initially explored via modelling based on the reactions given in Eqns. 1 and 2. This precursor is then converted to the diazonium derivative [n-Bu$_4$N]$_3$[PW$_{11}$O$_{39}${Sn(C$_6$H$_4$)C≡C(C$_6$H$_4$)N$_2^+$}] ([n-Bu$_4$N]$_3$K^W$_{Sn}$[N$_2^+$], (Figure 1(b)) which is then subsequently grafted onto the GC electrode as K^W$_{Sn}$[-]$^{4-}$-grafted (Figure S1). Thus, the thermodynamics and electrode kinetics for reduction of K^W$_{Sn}$[-]$^{4-}$ is evaluated according to Eqns. 3 and 4 using modelling relevant to this surface confined material.

$$K^W{}_{Sn}[N_3C_4H_{10}]^{4-}{}_{(soln)} + e^- \leftrightarrows K^W{}_{Sn}[N_3C_4H_{10}]^{5-}{}_{(soln)} \qquad (1)$$

$$K^W{}_{Sn}[N_3C_4H_{10}]^{5-}{}_{(soln)} + e^- \leftrightarrows K^W{}_{Sn}[N_3C_4H_{10}]^{6-}{}_{(soln)} \qquad (2)$$

$$K^W_{Sn}[-]^{4-}_{(grafted)} + e^- \leftrightarrows K^W_{Sn}[-]^{5-}_{(grafted)} \qquad\qquad (3)$$

$$K^W_{Sn}[-]^{5-}_{(grafted)} + e^- \leftrightarrows K^W_{Sn}[-]^{6-}_{(grafted)} \qquad\qquad (4)$$

Figure 1. Structural representation of (a) the precursor functionalized phosphotungstate POM $K^W_{Sn}[N_3C_4H_{10}]^{4-}$ used in solution phase electrochemical studies and (b) $K^W_{Sn}[N_2^+]^{3-}$ used for grafting to a GC electrode via the terminal diazonium group.

Electrografting of the related diazonium functionalized POMs $[PMo_{11}O_{39}\{Sn(C_6H_4)C\equiv C(C_6H_4)N_2^+\}]^{3-}$ [2] and $[PW_{11}O_{39}\{Ge(C_6H_4)C\equiv C(C_6H_4)N_2^+)\}]^{3-}$ [3] has been used to prepare chemically modified GC or silicon surfaces. Studies of the electron transfer kinetics of the functionalized POM grafted onto GC or silicon have been reported by traditional DC cyclic voltammetry [3, 22] using the separation in the peak reduction and oxidation potentials for the first one electron reduction process as a function of scan rate with reference to Laviron theory [30] used for quantification. Electrode kinetic studies with the solution soluble $[PW_{11}O_{39}\{Ge(C_6H_4)C\equiv C(C_6H_4)(N_3C_4H_{10})\}]^{4-}$ ($K^W_{Ge}[N_3C_4H_{10}]^{4-}$) also have been undertaken by linear sweep voltammetry which are based on comparison of the dependence of the reduction peak potential on scan rate [31]. Thus, parameterisation in these studies with solution soluble and surface confined POMs is derived from analysis of peak potentials. This very restricted use of only one or two data points selected from the extensive current-potential profile collected experimentally, means that information related to the shape of the voltammogram does not form part of the quantitative data analysis protocol, which minimises prospects for identifying nuances or non-idealities associated with the voltammetry.

In this study, the more sophisticated technique of Fourier transformed alternating current voltammetry (FTACV) is introduced to characterize the reduction of $K^W_{Sn}[N_3C_4H_{10}]^{4-}$ in the solution phase at GC, Au and Pt electrodes and $K^W_{Sn}[-]^{4-}$ grafted onto a GC electrode. This method allows all data in very

extensive sets collected in the experiments to be used in the parameterisation exercise, thereby allowing subtle departures from the theory predicted using the Butler-Volmer electron transfer model to be more readily detected. The thermodynamic and electrode kinetic parameters associated with reduction of $K^W_{Sn}[N_3C_4H_{10}]^{4-}$ in solution and surface confined $K^W_{Sn}[-]^{4-}$ are estimated with FTACV by comparing theoretical predictions based on MECSim [32] software derived simulated data with experimental data using both experimenter based heuristic and computationally supported data optimisation methods. Manual comparisons of simulated and experimental data are undertaken in the heuristic approach and the decision as to when the best fit data has been achieved is made by the experimenters on the basis of their expertise in voltammetry and data analysis. Knowledge from the tedious heuristic approach helps establish the range of variables that have to be searched in the computer assisted data optimization approach [33, 34]. Unlike the outcome of the heuristic approach, parameters derived from the data optimised analysis approach are independent of experimenter bias. However, an experienced electrochemist may more readily detect systematic departures of experimental data from theoretical predictions than by routinely implemented automated computational assessment as indeed applies in this study.

2. Experimental Section:

2.1 Reagents and solvents: The functionalized Keggin POM, $[n\text{-}Bu_4N]_4[PW_{11}O_{39}\{Sn(C_6H_4)C\equiv C(C_6H_4)(N_3C_4H_{10})\}]$ ($[n\text{-}Bu_4N]_4K^W_{Sn}[N_3C_4H_{10}]$) was prepared by a literature method [35]. Ferrocene (Fc, 98%, Sigma-Aldrich), Al_2O_3 (Buehler), trifluoroacetic acid (Sigma-Aldrich), diethylether (Merch-KGaA, Germany, 99.5%), dimethylformamide (DMF) and ethanol (96%, Merck) were used as provided by the manufacturer. Acetonitrile (CH_3CN, 99.9%, Sigma-Aldrich) was dried over molecular sieves. Tetrabutylammonium hexafluorophosphate ($[n\text{-}Bu_4N][PF_6]$, 98%, Sigma-Aldrich) and tetrabutylammonium bromide (Bu_4NBr, 98%, Sigma-Aldrich) were recrystallized from hot ethanol [36] and isopropanol (C_3H_8O, 99.5% Merck), respectively.

2.2 Synthesis of $[n\text{-}Bu_4N]_3[PW_{11}O_{39}\{Sn(C_6H_4)C\equiv C(C_6H_4)(N_2^+)\}]$ ($[n\text{-}Bu_4N]_3K^W_{Sn}[N_2^+]$): 40.9 mg of $[n\text{-}Bu_4N]_4K^W_{Sn}[N_3C_4H_{10}]$ (0.010 mmol) was dissolved in 2 mL of dried acetonitrile. 3.8 μL of

trifluoroacetic acid ($C_2HF_3O_2$, 0.050 mmol) was then added with stirring at room temperature for 10 minutes. A brown solid was removed by filtration of the yellow solution and 64.5 mg of Bu_4NBr was added to the filtrate. The required product was precipitated by mixing the filtrate with diethyl ether and collected, dried and stored under vacuum.

2.3 Electrochemical instrumentation and procedures: CH Instruments 700E and home built FTACV [37] electrochemical workstations were used to undertake DC cyclic and FTAC voltammetric experiments, respectively. In the FTACV, a sinusoidal wave having an amplitude ($\Delta E = 80$ mV) and frequency (f) of 9.02 Hz was superimposed onto the DC ramp. Resolution of the AC current-time data into aperiodic DC and AC harmonics was undertaken using Fourier transform based mathematical tools as described elsewhere [37]. All voltammetric experiments were carried out in a standard 3-electrode electrochemical cell at 22 ± 2° C under an inert environment achieved by conducting the experiments inside a dry box. Before grafting and prior to each electrochemical experiment, the GC electrode was polished on a polishing pad with an aqueous aluminium oxide (Al_2O_3, 0.3 µm) slurry, washed sequentially with water and acetone, and then dried under N_2. The same pre-treatment procedure also was applied to the Au and Pt electrodes. Pt wire and Pt wire inside a capillary tube were employed as counter and quasi-reference electrodes, respectively.

The electroactive areas (A) of the bare electrodes with a nominal diameter of 1.0 mm were estimated from the dependence of the peak current (I_P^{ox}) for the reversible $Fc^{0/+}$ oxidation process on scan rate using a 1.0 mM Fc solution in CH_3CN (0.10 M [n-Bu_4N][PF_6]) and the Randles-Sevcik equation (Eq. 5) [38] with a known diffusion coefficient ($D = 2.4 \times 10^{-5}$ cm^2 s^{-1}) for ferrocene [39] That is, values of parameters such as number of electrons transferred (n), A, scan rate (v), D, bulk concentration (C), temperature (T), Faraday's constant (F) and the universal gas constant (R) contained in Eq. 5 were assumed to be known and with mass transport occurring by liner diffusion [40]. On this basis, $A = 8.0 \times 10^{-3}$ cm^2 for GC, $A = 8.1 \times 10^{-3}$ cm^2 for Au and, $A = 8.0 \times 10^{-3}$ cm^2 for Pt.

$$I_{\mathrm{p}} = 0.4463nFA(nFDv/RT)^{1/2}C \tag{5}$$

The value of diffusion coefficient of $K^W_{Sn}[N_3C_4H_{10}]^{4-}$ of 6.3×10^{-6} cm^2 s^{-1} was calculated from the dependence of the peak current (I_P^{red}) on v and use of the Randles-Sevcik equation [38] for reduction of a 0.50 mM POM solution in CH_3CN containing 0.10 M [n-Bu$_4$N][PF$_6$] as the supporting electrolyte.

In order to establish if spontaneous adsorption of $K^W_{Sn}[N_3C_4H_{10}]^{4-}$ occurs and may be the origin of some discrepancies detected between simulated and experimental solution phase voltammetric data, freshly polished GC, Au and Pt electrodes were dipped into an acetonitrile solution containing 0.50 mM $K^W_{Sn}[N_3C_4H_{10}]^{4-}$ and 0.10 M [n-Bu$_4$N][PF$_6$] for at least five minutes. Electrodes were removed from the solution, sonicated in acetonitrile, rinsed carefully with acetone and dried under a nitrogen flow. Voltammetric experiments were then undertaken with these electrodes placed in CH_3CN containing only 0.10 M [n-Bu$_4$N][PF$_6$] electrolyte to detect the possible presence of surface attached POMs that had been adsorbed at open circuit potential. Analogous experiments were undertaken after the potential of the electrodes had been held at a value between the two $K^W_{Sn}[N_3C_4H_{10}]^{4-/5-/6-}$ processes for 0, 30, 60 or 120 s to ascertain if POM surface confinement occurred after reduction of $K^W_{Sn}[N_3C_4H_{10}]^{4-}$ to $K^W_{Sn}[N_3C_4H_{10}]^{5-}$.

Electrochemical quartz crystal microbalance (EQCM) experiments used to detect mass changes accompanying the voltammetry were undertaken with a 13.7 mm diameter ($A = 0.205$ cm^2) gold coated quartz crystal (oscillation frequency = 8.0 MHz) electrode using a CH Instruments 400B electrochemical workstation that supports EQCM experiments. The reference and counter electrodes in the EQCM measurements were again Pt wires.

Calibration of the potential of the Pt quasi-reference electrode was undertaken by reference to the IUPAC recommended $Fc^{0/+}$ process [40] under conditions of cyclic voltammetry and assuming its reversible potential is equal to the mid-point potential (average of oxidation and reduction peak potentials).

2.4 Electrografting of GC electrode surface: Grafting of the diazonium derivative [2] to the GC electrode surface was achieved via cyclic voltammetry (see Figure S2) of 1.0 mM of $K^W_{Sn}[N_2^+]^{3-}$ in

CH$_3$CN (0.10 M [n-Bu$_4$N][PF$_6$]) on a freshly polished GC electrodes over the potential range of -0.3 and -1.050 V vs Fc$^{0/+}$ with a scan rate of 0.100 V s^{-1}. Six cycles of potential were used to achieve close to a monolayer coverage. The grafted electrode was ultrasonicated in DMF and then CH$_3$CN (5 min each) to remove loosely attached material and dried under nitrogen. This surface grafted electrode was then used as the working electrode in subsequent voltammetric experiments in CH$_3$CN with 0.10 M of [n-Bu$_4$N][PF$_6$] present as the supporting electrolyte.

2.5 Theoretical analysis of AC voltammetry: All simulations were undertaken with the Monash University Simulation package MECSim [32]. Details of the theory used for simulation of solution phase FTAC voltammetry with mass transport by linear diffusion as applies to Eqns. 1 and 2 are available in the literature [41]. Simulation of the diffusionless surface confined voltammetry of the grafted POM was undertaken as described in the literature [42, 43]. In both scenarios, the Butler-Volmer model of electron transfer applied to a quasi-reversible process was used. This requires the incorporation of three (E^0, k^0, α) parameters for each electron transfer step, with units of k^0 being cm s^{-1} and s^{-1} for the solution soluble and grafted cases respectively. Neither thermodynamic nor kinetic dispersion that can occur with surface confined reactions [44, 45] were included in the simulation.

Ion-pairing chemistry reactions coupled to electron transfer were assumed to be diffusion controlled and hence reversible and subject to a solely thermodynamic description. On this basis, the unknown ion-pairing equilibrium constants effectively have been combined with the E^0 which implies that reported E^0, k^0, α values represent only apparent or E^0_{app}, k^0_{app} and α_{app} values. No double layer correction was applied to the electrode kinetics.

For the surface confined process, the Langmuir adsorption isotherm model was used. This adsorption isotherm implies that all surface confined grafted POM moieties present in monolayer or sub-monolayer coverage are electrochemically identical in their behaviour and act independently of each other. Use of the Langmuir relationship also requires that no dissolution of surface bound POM occurs during the course of the voltammetric experiment. The surface concentration (Γ) of K$^W_{Sn}$[-]$^{4-}$ in

moles cm^{-2} was calculated from the charge Q in coulomb transferred during the first surface confined reduction process as given by Eqn. 6.

$$\Gamma = N/A = Q/nFA \tag{6}$$

where N is number of moles of the electroactive species.

Modelling uncompensated resistance (R_u) via Ohm's law required the inclusion of this parameter in the simulations. The value of R_u used assumes a simple R_uC_{dl} time constant applies at potentials prior to the onset of POM reduction. Other parameters present in the simulation model such as AC amplitude, frequency, DC scan rate, electrode area, temperature were assumed to be accurately known.

Double layer capacitance (C_{dl}) was evaluated from the background current in the potential region of the fundamental harmonic of the FTACV response (Figure S3) where faradaic current is absent. A non-linear model was used to model the potential dependence of C_{dl} as in Eqn. 7 [46]

$$C_{dl}(t) = c_0 + c_1E(t) + c_2E(t)^2 + c_3E(t)^3 + c_4E(t)^4 \tag{7}$$

In this equation, the nonlinearity of the capacitor is defined by the coefficients c_0, c_1, c_2, c_3, and c_4 and the time dependant potential is designated by $E(t)$. However, it will emerge that the background current, particularly at the POM modified electrode, exhibits even more complicated behaviour than predicted by this model, although conveniently, second and higher order AC harmonics are essentially devoid of background current, as predicted by the model.

As in previous papers [47, 48], automated computationally supported comparison of experimental and simulated data in the data optimisation exercises were undertaken using a least squares (LS) function (Eqn. 8) to estimate E^0, k^0 and α values obtained with the best fit of theory to experimental data.

$$LS = \left[1 - \left(\sum_{h=2}^{6}\sqrt{\frac{\sum_{i=1}^{N}\left[\left(f_h^{exp}(t_i) - f_h^{sim}(t_i)\right)^2\right]}{\sum_{i=1}^{N}f_h^{exp}(t_i)^2}}\right)/5\right] \times 100\% \tag{8}$$

where $f^{\exp}(t_i)$ and $f^{\sim}(t_i)$ characterize the experimental and simulated functions, respectively, h is the order of an individual AC harmonic component, H is the total number of AC harmonic components and N is the number of data points. Here, only the 2nd to 6th harmonics were employed for optimisation so the influence of background current present in the aperiodic DC and fundamental harmonic could be ignored in the optimisation exercise

3. Result and Discussion:

3.1 DC cyclic voltammetric studies for the solution soluble and surface confined POMs

Figure 2 shows a DC cyclic voltammogram at a GC electrode for reduction of $K^W_{Sn}[N_3C_4H_{10}]^{4-}$ over the potential range of about -0.1 to -1.7 V vs $Fc^{0/+}$. No reduction response associated with the side chain is evident prior to the $K^W_{Sn}[N_3C_4H_{10}]^{4-/5-}$ process observed at about -1.4 V vs $Fc^{0/+}$.
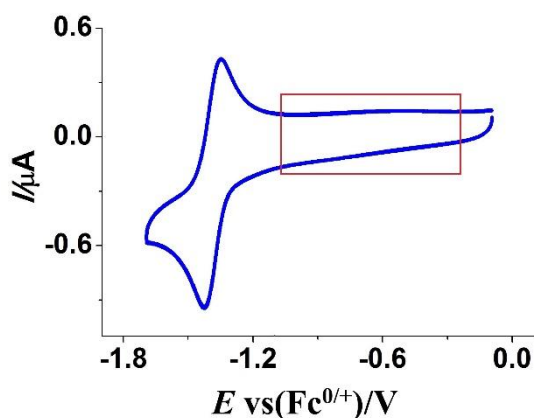
Figure 2. DC Cyclic voltammetry of $K^W_{Sn}[N_3C_4H_{10}]^{4-}$ in CH_3CN (0.10 M [n-Bu$_4$N][PF$_6$]) at a scan rate of 0.100 V s^{-1} with a GC electrode over the potential range of about -0.10 to -1.7 V vs $Fc^{0/+}$ which covers the region where grafting with the diazonium derivative (red marked area) and the first $K^W_{Sn}[N_3C_4H_{10}]^{4-/5-}$ process occur.

DC Cyclic voltammograms for a 0.50 mM $K^W_{Sn}[N_3C_4H_{10}]^{4-}$ solution and the surface confined grafted $K^W_{Sn}[-]^{4-}$ at a GC electrode recorded over a wider potential range than in Figure 2 are provided in Figure 3. In the former case, three reduction processes are observed at a GC electrode (Figure 3 (a-i)).

11

The first two, which are assigned to $K^W_{Sn}[N_3C_4H_{10}]^{4-/5-}$ and $K^W_{Sn}[N_3C_4H_{10}]^{5-/6-}$ processes and are of interest in this study, are well defined and chemically reversible since the magnitudes of the ratios of the reduction to oxidation peak currents are close to unity. Consequently, their mid-point potentials, $(E^p_{ox} + E^p_{red})/2$, can be equated to the reversible potential, E^0, values of -1.390 and -1.843 V vs $Fc^{0/+}$, respectively. These processes also can be classified as essentially reversible or close to reversible in the electrochemical sense since their peak-to-peak separation ($E^{red}_P - E^{ox}_P$) values of ~60 mV, uncorrected for IR_u drop, are close to the theoretically predicted value of 56.4 mV for a reversible one-electron transfer process at 22° C [38]. The third most negative process at about -2.4 V vs $Fc^{0/+}$ at the GC electrode is chemically irreversible and not considered further.

Interestingly, the shapes of the processes for reduction of $K^W_{Sn}[N_3C_4H_{10}]^{4-}$ detected at Au (Figuren3a-ii) and Pt (figure 3a-iii) electrodes differ significantly from those at the GC electrode. The first process at these metal electrodes is assigned as quasi-reversible by traditional forms of analysis of DC cyclic voltammograms on the basis of their much larger ($E^{red}_P - E^{ox}_P$) separations but identical mid-point potentials relative to values of these parameters at the GC electrode. In contrast, the second $K^W_{Sn}[N_3C_4H_{10}]^{5-/6-}$ process at the Au electrode is observed at a significantly more negative potential (mid-point potential approximately -1.94 V) than at the GC electrode while this process is ill-defined at Pt, indicating additional complexity relative the quasi-reversible assignment scenario. Thus modelling these processes with the Butler-Volmer relationship will not be appropriate.

With the grafted GC electrode, the cyclic voltammetry (Figure 3b), contains $K^W_{Sn}[-]^{4-/5-}$ and $K^W_{Sn}[-]^{5-/6-}$ reduction processes with mid-point potentials of -1.450 V and -1.922 vs $Fc^{0/+}$, respectively The shapes of both these diffusionless processes are symmetrical unlike those for the diffusion-controlled solution phase reactions, as expected theoretically. The germanium analogue of the tungsten, $K^W_{Ge}[-]^{4-}$ [3] grafted GC electrode also exhibits two well resolved symmetrically shaped reduction processes.
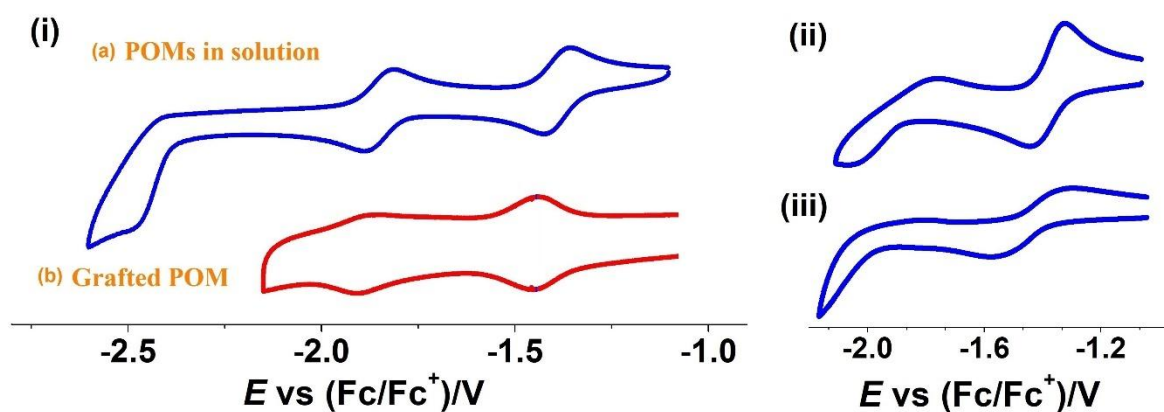
Figure 3. DC cyclic voltammetry of $K^W_{Sn}[N_3C_4H_{10}]^{4-}$ at a bare (ai) GC, (aii) Au and (aiii) Pt electrodes and (b) at a $K^W_{Sn}[-]^{4-}$-grafted GC electrode at a scan rate of 0.100 V s^{-1} in CH$_3$CN (0.10 M [n-Bu$_4$N][PF$_6$]).

A summary of $\Delta E_p(E^p_{ox} - E^p_{red})$ and E^0 values determined by DC cyclic voltammetry for dissolved $K^W_{Sn}[N_3C_4H_{10}]^{4-}$ and grafted $K^W_{Sn}[-]^{4-}$ are provided in Table 1 and compared with those for related polyoxomolybdate $[PMo_{11}O_{39}\{Sn(C_6H_4)C{\equiv}C(C_6H_4)(N_3C_4H_{10})\}]^{4-}$ ($K^{Mo}_{Sn}[N_3C_4H_{10}]^{4-}$) [2] and polyoxotugstate $K^W_{Ge}[N_3C_4H_{10}]^{4-}$ [3] compounds.

Table 1. Summary of DC cyclic voltammetric data obtained at a scan rate of 0.100 V s^{-1} in CH$_3$CN (0.10 M [n-Bu$_4$N][PF$_6$]).

POM type	Electrode	E^0_{app1}	E^0_{app2}	E^0_{app1}	E^0_{app2}	ΔE_{P1}	ΔE_{P2}
		V vs SCE		V vs Fc$^{0/+}$ [a]		mV	
$K^W_{Sn}[N_3C_4H_{10}]^{4-}$	Bare-GC			-1.390	-1.843	63	67
	Bare-Au			-1.400	-1.94[b]	103	310[c]
	Bare-Pt			-1.400[c]	[d]	310[c]	[d]
	Grafted-GC ($K^W_{Sn}[-]^{4-}$)			-1.450	-1.922	13	37
$K^W_{Ge}[N_3C_4H_{10}]^{4-}$	Bare-GC	-0.990	-1.460	-1.300	-1.770	65$\pm$5	65$\pm$5
	Grafted-GC ($K^W_{Ge}[-]^{4-}$)	-1.010	-1.500	-1.310	-1.800	30	60
$K^{Mo}_{Sn}[N_3C_4H_{10}]^{4-}$	Bare-GC	-0.500	-0.920	-0.810	-1.230	--	--
	Grafted-GC ($K^{Mo}_{Sn}[-]^{4-}$)	-0.550	[d]	-0.860	[d]	72[e]	[d]

[a]Converted to Fc$^{0/+}$ scale [38, 49] when required

In terms of electrode kinetics, the following qualitative cncusions might be made from data in Table 1. The ΔE_{p1} value of 63 ± 2 mV at a GC electrode for the $K^W_{Sn}[N_3C_4H_{10}]^{4-/5-}$ reduction processes in solution phase at a scan rate of 0.100 V s^{-1} approaches the theoretically predicted value for ΔE_p of 56.4 mV for a reversible one-electron process. The difference may be attributed to the presence of a small amount of Ohmic IR_u drop, so that on this DC time scale this process may be regarded as reversible, within experimental error. ΔE_{p2} is slightly larger for the second process $(\Delta E_{p2} = 67 \pm 2 \text{ mV})$ implying that $k_1^0 > k_2^0$ and that the second process is quasi-reversible rather than reversible. The much larger ΔE_p values for the KWSn[-]$^{4-/5-}$ process at Au and Pt than at GC electrodes implies that $k_{GC}^0 > k_{Au}^0 > k_{Pt}^0$.

The D value of 6.3×10^{-6} cm^2 s^{-1}) for $[K^W_{Sn}[N_3C_4H_{10}]^{4-}$ was estimated from the DC voltammetric peak reduction current for the $K^W_{Sn}[N_3C_4H_{10}]^{4-/5-}$ process at a GC electrode as described in the Experimental Section. The D value for the germanium analogue in CH$_3$CN is reported to be 9.3×10^{-6} cm^2 s^{-1} [3].

The first reduction process at the $K^W_{Sn}[-]^{4-}$-grafted GC electrode in contact with CH$_3$CN (0.10 M [n-Bu$_4$N][PF$_6$]) has a ΔE_{p1} value of 13 ± 2 mV at a scan rate of 0.100 V s^{-1} which differs slightly from the value of zero predicted theoretically for a reversible process [50]. On the other hand, the much larger value of ΔE_{p2} of 37 ± 2 mV is well removed form that predicted for the reversible value implying a much slower electron transfer rate for this process, relative electrode to the first one.

The E^0 values [2] $K^{Mo}_{Sn}[N_3C_4H_{10}]^{4-}$ in solution phase and for the $K^{Mo}_{Sn}[-]^{4-}$ grafted-GC and are considerably less negative than for the W derivatives studied in this paper (Table 1). This is usually the case in POM electrochemistry and is attributed to the significantly lower position of the LUMO energy for a Mo based POM compared to its W analogue, also noting that the HOMO-LUMO gap is

~2 eV for molybdates which is smaller than ~2.8 eV for tungstates [51]. The potentials for the germanium analogues of the tin derivatives in both solution and surface confined (grafted electrode) phases are considered to be similar when uncertainties in conversion of literature data reported vs SCE to the $Fc^{0/+}$ scale are taken into account. This reflects the fact that this change of a single side chain atom is less significant in terms of redox thermodynamics than when all W are replaced by all Mo in the polyoxometalate core framework. Differences in values of E_1^0 and E_2^0 are very similar for all compounds in both solution soluble and grafted cases, again as might be expected.

In three experiments undertaken in this study, the POM surface coverage, Γ, was estimated from the charge calculated from DC voltammetric experiments to be 6.2×10^{-11}, 8.8×10^{-11} and 10×10^{-11} mol cm^{-2} which approaches the value estimated for a monolayer of immobilized polyoxomolybdate analogue, $K^{Mo}_{Sn}[-]^{4-}$ [2] on a GC electrode, although it is noted that multilayer formation could arise by aryl radicals reacting with already grafted aryls [52].

## 3.2 FTACV voltammetric characterization of the $K^{W}_{Sn}[N_3C_4H_{10}]^{4-/5-/6-}$ processes

E^0, k^0 and α values were quantified by comparison of experimental and simulated FTACV data modelled by use of the Butler Volmer relationship, although from now on they will be referred to as E^0_{app}, k^0_{app} and α_{app} since they neglect ion-pairing and are regarded as apparent values (see above).

The k^0_{app}, and α_{app} values associated with the $K^{W}_{Sn}[N_3C_4H_{10}]^{4-/5-}$ process in acetonitrile containing 0.10 M [n-Bu$_4$N][PF$_6$] at the bare GC electrode were initially determined using heuristic form of data analysis of the FTACV data obtained with 0.20 mM $K^{W}_{Sn}[N_3C_4H_{10}]^{4-}$. In this exercise, E^0_{app} = -1.390 V, derived from the mid-point potential in DC cyclic voltammetry (see above), was employed as a known rather than estimated parameter value. Simulated data containing variable combinations of k^0_{app}, and α_{app} were compared with experimental data and adjustments to simulated data constantly undertaken until the experimenter decided that the "best fit" had been achieved. Parameters reported by this tedious and subjective method are included in Table 2.

A comparison of the FTACV experimental voltammetry for 0.20 mM $K^W_{Sn}[N_3C_4H_{10}]^{4-}$ at a GC electrode and the simulated voltammetry achieved heuristically as the "best fit" in this work is shown in Figure 4(i). Good, but not perfect agreement between experimental and simulated data for the third and higher order AC harmonics is evident in this outcome of the data analysis exercise undertaken by the experimenter. Clearly the background current is not perfectly matched in either the DC, or fundamental or second harmonic AC responses. Additionally, the experimental faradaic responses are not quite as symmetrical with respect to reduction and oxidation components as the ones simulated using the Butler-Volmer model. In the heuristic form of data analysis, and to address this asymmetry issue, matching of reduction component was chosen in the simulation-experimental comparisons to obtain the "best fit" and enumerate the k^0_{app}, and α_{app} parameters. This achieved an almost perfect fit of this set of data for all the higher order harmonics based on visual inspection. The assumption made by the experimentalist in choosing this modus operandi is that non-ideality in the modelling is negligible in the data derived at short times from the reduction component of the experiment with features not accommodated in the model having a small impact at longer experimental times relevant to data collected in the oxidation component. Support for implementing data analysis based on this hypothesis is provided below, but clearly a different experimentalist may have chosen to undertake a different approach in the heuristic method and generate apparently different values of k^0_{app}, and α_{app}.

The values of k^0_{app} and α_{app} must be regarded as unreliable when determined by FTACV or any other method when they lie at or very close to the reversible limit where Nernstian rather than Butler-Volmer theory may be more appropriate. With 0.20 mM $K^W_{Sn}[N_3C_4H_{10}]^{4-}$, the heuristically estimated k^0_{app} value of 0.058 cm s^{-1} and α_{app} of 0.50 at 9.02 Hz are derived from good agreement of experimental results with simulated data that lie well below that predicted for a simulated reversible process (Figure 4(i)) so modelling on the basis of a kinetically controlled quasi-reversible reaction is concluded to be appropriate.
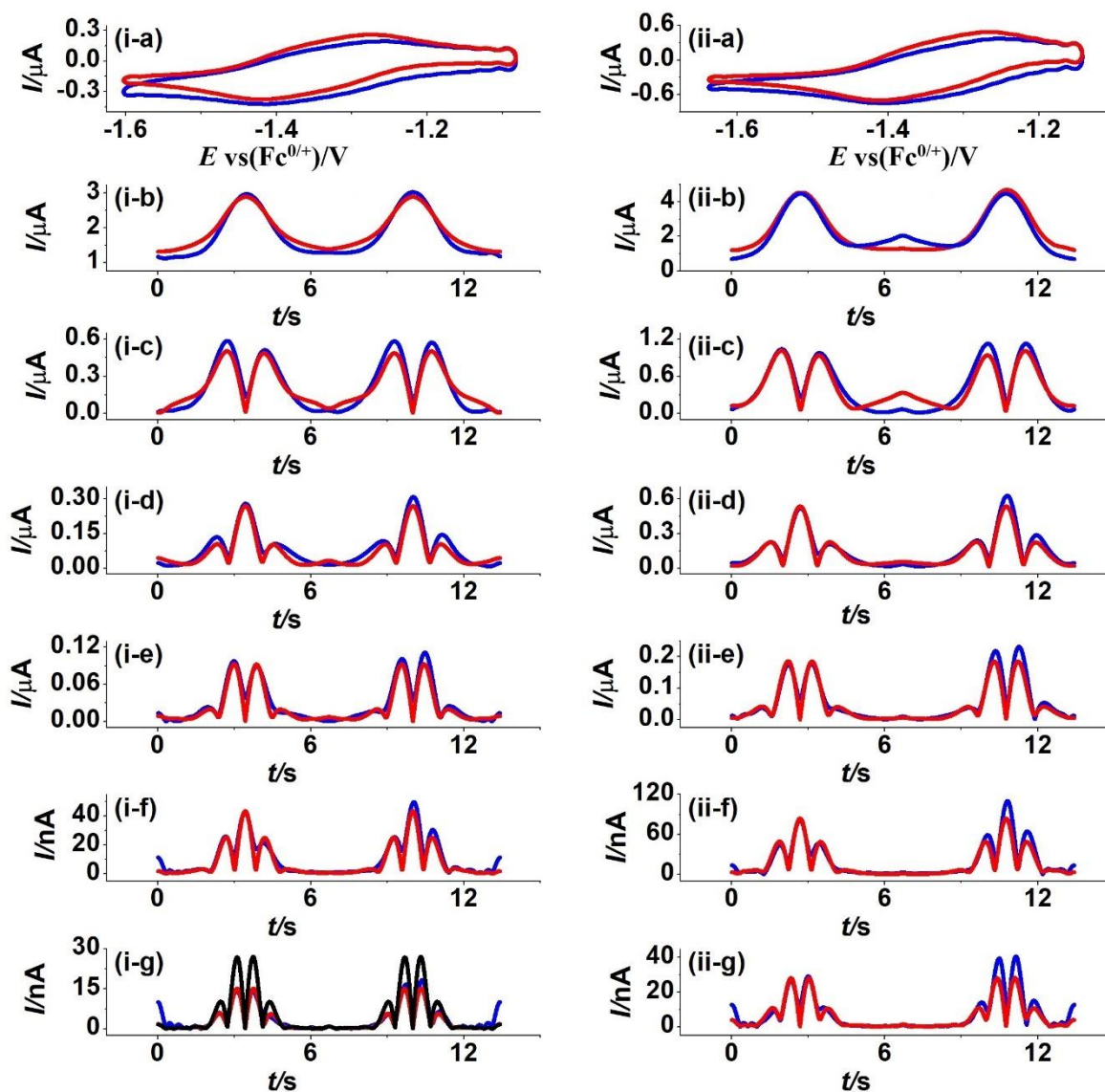
Figure 4: Heuristic comparison of simulated (red) and experimental (blue) FTAC voltammetric data for the $K^W_{Sn}[N_3C_4H_{10}]^{4-/5-}$ process, obtained with (i) 0.20 and (ii) 0.50 mM $K^W_{Sn}[N_3C_4H_{10}]^{4-}$ in CH_3CN (0.10 M [n-Bu$_4$N][PF$_6$]) at a bare GC electrode. $\Delta E = 80$ mV, $f = 9.02$ Hz and $v_{0.20\,mM} = 0.078$ V s^{-1} and $v_{0.50\,mM} = 0.075$ V s^{-1}. (a) DC component, (i and iib, c, d, e, f, g) 1st to 6th harmonic components where parameters used in the simulations are given in Table 2, (i-g) comparison of experimental data with that for the 6th harmonic component simulated for a reversible process (black).

Heuristic electrode kinetic parameterisation using a higher concentration (0.50 mm) of K^w_{an} [$N_3C_4H_{10}$]$^{4-}$ also was investigated by the FTACV technique as shown in Figure 4(ii), and again emphasising the reduction component of the data. Discrepancies associated with modelling of the

background current are now relatively less important at the higher POM concentration, but asymmetry not predicted in the faradaic reduction and oxidation components is slightly more pronounced than with the lower 0.20 mM POM concentration. Nevertheless, results presented in Table 2 on the basis of heuristic analysis with incorporation of judgemental input from an experienced electrochemist show that as theoretically required, the electrode kinetic parameters are concentration independent as theoretically predicted. This outcome also implies that IR_u drop has been correctly modelled.

Table 2. Electrode kinetic parameters[a] derived from heuristic and computer-based comparison of simulated and experimental FTACV data at 9.02 Hz at a bare GC, Au and Pt electrode for the $K^W_{Sn}[N_3C_4H_{10}]^{4-/5-}$ process in CH_3CN (0.10 M $[n\text{-}Bu_4N][PF_6]$).

Electrode	Conc (mM)	Simulation method	R_u (Ω)[b]		E^0_{app} V vs Fc$^{0/+}$	k^0_{app} (cm s^{-1})	α_{app}	LS %
GC	0.20	Heuristic	510		-1.390	0.058[c]	0.50	
		Automated		Range	-1.395 to -1.385	0.040 to 0.095	0.40 to 0.70	
				Estimated	-1.390	0.075[d]	0.42	84
	0.50	Heuristic	599		-1.390	0.056[c]	0.50	
		Automated		Range	-1.397 to -1.385	0.045 to 0.095	0.40 to 0.70	
				Estimated	-1.391	0.075[d]	0.42	87
Au	0.20	Heuristic	521		-1.390	0.016	0.50	
		Automated		Range	-1.396 to -1.387	0.005 to 0.030	0.40 to 0.70	
				Estimated	-1.394	0.014	0.43	75
Pt	0.20	Heuristic	511		-1.390	0.009 to 0.031[e]	0.43	
		Automated		Range	-1.395 to -1.386	0.002 to 0.040	0.40 to 0.70	
				Estimated	-1.394	0.022	0.43	69

[a] Other parameters used in the simulations are: $A_{GC} = 8.0 \times 10^{-3}$ cm^2, $A_{Au} = 8.1 \times 10^{-3}$ cm^2, $A_{Pt} = 8.0 \times 10^{-3}$ cm^2, $\Delta E = 80$ mV, $D = 6.3 \times 10^{-6}$ cm^2 s^{-1}, $T = 295$ K, $v_{0.20\ mM} = 0.078$ V s^{-1} and $v_{0.50\ mM} = 0.075$ V s^{-1} with GC electrode, $v_{Au\ and\ Pt} = 0.078$ V s^{-1}, $f = 9.02$ Hz.

[b] vary due to slight difference in electrode arrangement in cell.

[c] determined from analysis of the reduction component of data only.

[d] derived from use of all data even though asymmetry is present in reduction and oxidation components.

[e] apparently harmonic dependent kinetics.

Parameter values estimated from the heuristic data analysis exercise allow the search of parameter space to be constrained efficiently and sensibly so as to minimise the computational time required in automated data optimisation analysis. Thus, E_{app}^0 = -1.395 to -1.385 V, k_{app}^0 = 0.040 to 0.095 cm s^{-1}, α_{app} = 0.40 to 0.70 ranges were used for example in simulations undertaken in the computer aided data optimisation procedure for the first reduction process with 0.20 mM $K^W{}_{Sn}[N_3C_4H_{10}]^{4-}$ obtained by FTACV at a frequency of 9.02 Hz. The ranges of parameters and resolution used for all simulations are included in Table 2. In this data optimisation exercise, least squares comparison of the experimental and simulated voltammograms, as was the case with the heuristic method, was restricted to the 2nd to 6th harmonics that contain negligible influence from the background current. Normally, the automated method, unless trained to be an intelligent expert system, would find the "best fit" based on lest squares outcomes using all data. Best fit values for E_{app}^0, k_{app}^0 and α_{app} parameters found via this automated computer assisted method using all data and not just data for the reduction component as used in the heuristic method of analysis are summarised in Table 2. While agreement between simulated and experimental FTAC voltammetry is again excellent, close inspection confirms that the small level of asymmetry is still not accommodated by theory. Variation in how the asymmetry is accommodated in the modelling lead to the data analysis dependent electrode kinetic parameters contained in Table 2. In particular, the data optimisation method using all data produces an α_{app} value of about 0.42 which is a result of the attempting to mimic the asymmetry, whereas an α_{app} value of 0.50 is deduced via heuristic analysis by confining data analysis solely to the reduction component. Furthermore, the automated method provides a slightly larger value of k_{app}^0 of around 0.075 relative to the value of 0.058 cm s^{-1} obtained via the heuristic approach. Significantly, restricting the data optimisation analysis to just the reduction component generates parameter values almost identical to those reported heuristically. It will emerge from studies descried below, that weighting data analysis in this manner can be justified and indeed having α_{app} value of close to 0.50 via this approach is intrinsically satisfying for the $K^W{}_{Sn}[N_3C_4H_{10}]^{4-/5-}$ process which should not involve significant structural change. This study illustrates the value of initially using heuristic approaches to enhance prosects of detecting potential modelling imperfections.

Both of the $K^W_{Sn}[N_3C_4H_{10}]^{4-/5-/6-}$ processes at GC electrode in solution phase also were parameterised using experimental data collected over a potential range that is sufficiently large to accommodate both reactions (Figure 5). Values derived from both heuristic (reduction component only) and automated data optimisation (all data used with parameter space ranges selected from heuristic results) from 0.20 and 0.50 mM solutions of $K^W_{Sn}[N_3C_4H_{10}]^{4-}$ are summarized in Table 3. Any influence of the cross redox reaction given in eqn. 9 was neglected in this modelling.

$$K^W_{Sn}[N_3(C_4H_{10})]^{4-} + K^W_{Sn}[N_3(C_4H_{10})]^{6-} \leftrightharpoons 2\ K^W_{Sn}[N_3(C_4H_{10})]^{5-} \qquad (9)$$
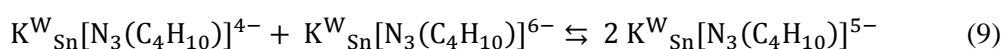
Clearly, the second $K^W_{Sn}[N_3C_4H_{10}]^{5-/6-}$ process is kinetically slower than first $K^W_{Sn}[N_3C_4H_{10}]^{4-/5-}$ process (*e.g.* $k^0_{app1} = 0.056$ cm s^{-1} versus $k^0_{app2} = 0.020$ cm s^{-1} for heuristic analysis for 0.20 mM POM data). This outcome is consistent with the suggestion based on the larger DC cyclic voltammetric peak-to-peak separations for the second process, where $\Delta E_{P2} = 67$ mV $> \Delta E_{P1} = 63$ mV (see Table 1). As would be anticipated, the asymmetry not predicted by theory again leads to data analysis method dependent elected kinetic parameter values. However, parameter estimates for the first process are independent of whether the data are collected independently of the second process or simultaneously with the second process.

k^0_{app} for the solution soluble Ge analogue of the Sn derivative at a GC electrode in CH$_3$CN has been reported[3] to be 0.064 cm s^{-1} (α_{app} assumed to be 0.50) for the $K^W_{Ge}[N_3C_4H_{10}]^{4-/5-}$ process via analysis of a plot of reduction peak potential versus scan rate obtained under conditions of linear sweep voltammetry [53] and hence similar to that for the $K^W_{Sn}[N_3C_4H_{10}]^{4-/5-}$ process.

The k^0_{app} value for the $K^W_{Sn}[N_3C_4H_{10}]^{4-/5}$ process is about three times slower than that for the α-$[S_2W_{18}O_{62}]^{4-/5-}$ process at a GC electrode under the same conditions [Md Anisur Rahman's unpublished work, Monash University, 2020. **Anis give this a reference number with DOI.** The long diazonium chain in the structure of $K^W_{Sn}[N_3C_4H_{10}]^{4-}$ may influence the rate of electron transfer kinetics by restricting the distance of closest approach of the POM to the electrode surface and lead to

slower electrode kinetic than for the fully symmetrical α-$[S_2W_{18}O_{62}]^{4-}$ POM, although differences in ion-paring and other factors also may play a role.
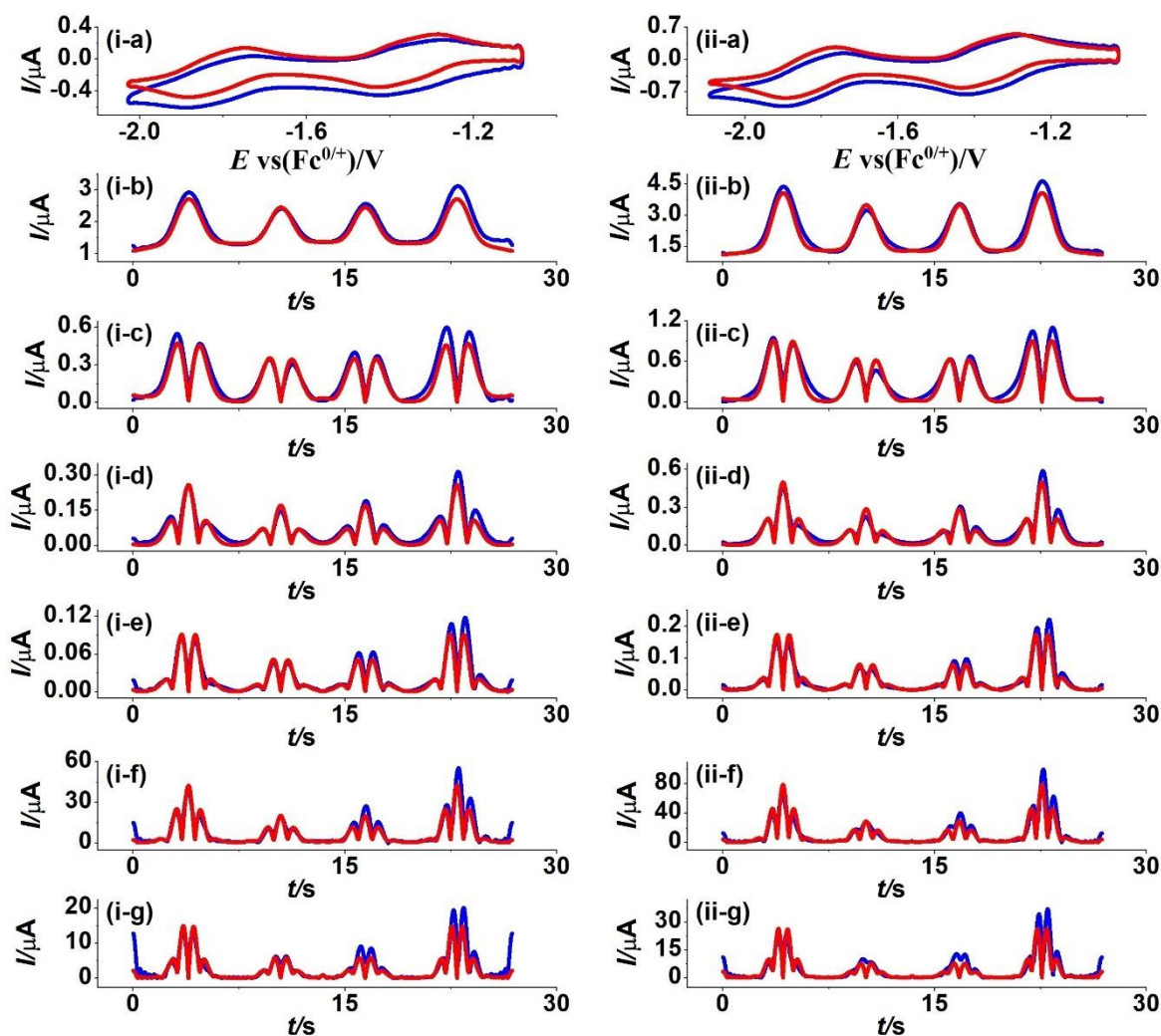
Figure 5: Heuristic comparison of simulated (red line) and experimental (blue line) AC voltammetric data for the $K^W_{Sn}[N_3C_4H_{10}]^{4-/5-/6-}$ process, obtained with (i) 0.20 mM and (ii) 0.50 mM $K^W_{Sn}[N_3C_4H_{10}]^{4-}$ in CH$_3$CN (0.10 M [n-Bu$_4$N][PF$_6$]) at a bare GC electrode. $\Delta E = 80$ mV, $f = 9.02$ Hz and $v_{0.20\ mM} = 0.071$ V s^{-1} and $v_{0.50\ mM} = 0.080$ V s^{-1}. (a) DC component, (b-g) 1st to 6th harmonic components.

Table 3. Electrode kinetic parameters [a] derived from the heuristic and computer-based comparison of simulated and experimental FTACV data at 9.02 Hz at a bare GC electrode for the $K^W_{Sn}[N_3C_4H_{10}]^{4-/5-}$ and $K^W_{Sn}[N_3C_4H_{10}]^{5-/6-}$ processes in CH_3CN (0.10 M [n-Bu$_4$N][PF$_6$]).

Conc (mM)	Simulation method	R_u (Ω)[b]		E^0_{app1}	E^0_{app2}	k^0_{app1}	k^0_{app2}	α_{app1}	α_{app2}	LS %
				V vs Fc$^{0/+}$		cm s^{-1}				
0.20	Heuristic	510		-1.390	-1.843	0.056[c]	0.020[c]	0.50	0.50	
	Automated		Range	-1.395 to -1.386	-1.847 to -1.840	0.040 to 0.095	0.005 to 0.045	0.40 to 0.70	0.40 to 0.70	
			Estimated	-1.387	-1.845	0.071[d]	0.023[d]	0.42	0.42	81
0.50	Heuristic	599		-1.390	-1.843	0.056[c]	0.016[c]	0.50	0.50	
	Automated		Range	-1.395 to -1.386	-1.847 to -1.839	0.040 to 0.085	0.005 to 0.045	0.40 to 0.70	0.40 to 0.70	
			Estimated	-1.387	-1.846	0.072[d]	0.018[d]	0.43	0.43	80

[a] Other parameters used in the simulations are: A_{GC} = 8.0 × 10^{-3} cm^2, ΔE = 80 mV, D = 6.3 ×10^{-6} cm^2 s^{-1}, T = 295 K, $v_{0.20\ mM}$ = 0.071 V s^{-1}, $v_{0.50\ mM}$ = 0.080 V s^{-1}, f = 9.02 Hz.

[b] vary due to slight differences in the electrode arrangement.

[c] determined from reduction component of data only

[d] derived from use of all data.

FTACV studies on the $K^W_{Sn}[N_3(C_4H_{10})]^{4-/5-}$ process at Au and Pt metal electrodes also were undertaken. As stated above, the electrode material dependency predicted on basis of peak-to-peak separations obtained in DC cyclic voltammetry (Table 1) is $k^0_{GC} > k^0_{Au} > k^0_{Pt}$, as reported with other POMs [25]. However, as at GC, FTACV data analysis of the voltammetry at the metal electrodes reveals nuances in the mechanisms relative to predictions based on a simple one-electron quasi-reversible process. Comparisons of simulated and experimental data for FTACV based on heuristic analysis are provided in Figure S5 for Au and Figure S6 for Pt, while parameters that are obtained from the heuristic and computer supported forms of data analysis used in this study are summarised in Table 2. Clearly, agreement between experimental and simulated data at Au and Pt are poorer than at the GC electrode. Furthermore, electrode kinetic parameters are even more strongly dependent on the method of data analysis.

Assuming the Butler-Volmer model is valid, the kinetics at GC ($k_{app1}^0 = 0.058$ cm s^{-1}) are faster than at Au ($k_{app1}^0 = 0.016$ cm s^{-1}) based on the heuristic approach and use of only the reduction component. However, there is significant uncertainty as to whether this model is even appropriate for analyses of data obtained with the Pt electrode. With Au, and unlike theoretical predictions, the oxidation current component is larger than reduction one as for GC case, but even more pronounced and a mismatch in background current in DC and fundamental harmonic components is evident. In the case of Pt, excellent agreement between experiment and theory is provided for the third harmonic ($k_{app1}^0 = 0.013$ cm s^{-1}) in Figure S6(ii) based on heuristic estimation, but use of this same rate constant to model lower and higher harmonics respectively overestimates and underestimates the current magnitudes significantly. That is, apparently harmonic dependant kinetics in the range of 0.0095 to 0.031 cm s^{-1} are observed at the Pt electrode (shown in Figure S6(i)) when best fits applied consecutively to fundamental to sixth harmonic AC data. Theoretically, of course, the rate constant should be harmonic independent. Modelling with Marcus-Hush theory as an alternative to the Butler-Volmer model was considered but did not produce superior fits to data. At Pt, the background current in DC aperiodic and fundamental harmonic components predicted theoretically also differ from that determined experimentally. Harmonic dependent location of potentials of peaks also are evident in theory-experiment comparisons. Finally, it is noted that even the shape of a conventional DC cyclic voltammogram at the Pt electrode does perfectly match theoretical predictions as also noted with the Fc$^{0/+}$ process at boron diamond electrodes when sp^2 graphite impurity provided complexity in the response [47]. Differences in experimental and theoretical data based on the Butler-Volmer model with mass transport by linear diffusion at Pt are so profound that parameterisation on this basis is not highly signfcant. Clearly, the voltammetry of K^W$_{Sn}$[N$_3$(C$_4$H$_{10}$)]$^{4-/5-}$ and K^W$_{Sn}$[N$_3$(C$_4$H$_{10}$)]$^{5-/6-}$ processes are more complex than predicted at all electrodes used, with the extent of non-ideality being in the order Pt > Au > GC.

3.3 Origin of discrepancies of experimental data and predictions based on Butler-Volmer electrode kinetic model:

Variable levels of non- conformance to the Butler-Volmer model of electron transfer were detected in the solution phase FTAC voltammetry of $K^W_{Sn}[N_3C_4H_{10}]^{4-}$ at GC, Au and Pt electrodes. One possible explanation for the anomalous behaviour is that reduction of $K^W_{Sn}[N_3C_4H_{10}]^{4-}$ to $K^W_{Sn}[N_3C_4H_{10}]^{5-}$ leads to modification of the electrode surface which could alter the shape and other characteristics of the voltammetry in a time or potential dependent manner not accommodated by the theory.

In principle, surface interaction of $K^W_{Sn}[N_3C_4H_{10}]^{4-}$ or $K^W_{Sn}[N_3C_4H_{10}]^{5-}$ with the electrode surface should lead to a mass change during the course of the voltammetry which can be detected by the EQCM method via a change in the oscillation frequency of a Au coated quartz crystal electrode [54]. Accordingly, the frequency (mass) change of a gold crystal working electrode was monitored during DC cyclic voltammetry undertaken in CH_3CN (0.10 M $[n\text{-}Bu_4N][PF_6]$) with and without 0.50 mM $K^W_{Sn}[N_3(C_4H_{10})]^{4-}$ at a scan rate of 0.050 V s^{-1} over the potential range covering the region where grafting (Figure 6(i-b)) occurs with the diazonium derivative $K^W_{Sn}[N_2^+]^{3-}$ at a GC electrode (see above) as well as the first $K^W_{Sn}[N_3(C_4H_{10})]^{4-/5-}$ process (Figure 6(i-a)). Although we have not prepared a grafted Au electrode in this study, Gooding et al [55-57] for example have shown that Au also provides an excellent surface for diazonium grafting.
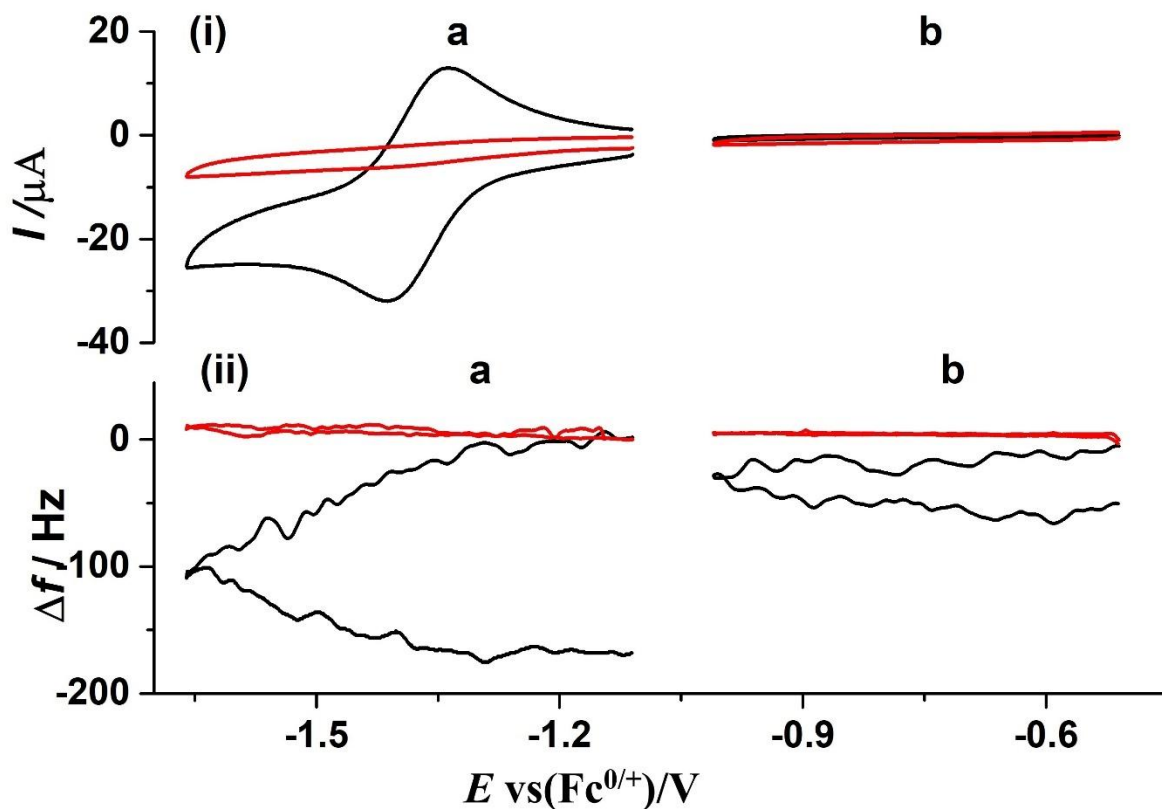
Figure 6. EQCM data obtained for 0.50 mM $K^W_{Sn}[N_3C_4H_{10}]^{4-}$ at a scan rate of 0.050 V s^{-1} with an Au quartz crystal electrode over the potential range covering the region where grafting (b) occurs with diazonium derivative and the first $K^W_{Sn}[N_3C_4H_{10}]^{4-/5-}$ process (a) occurs. (i) cyclic voltammetry (current versus potential) and (ii) frequency versus potential. (----) 0.50 mM $K^W_{Sn}[N_3C_4H_{10}]^{4-}$ in CH$_3$CN (0.10 M [n-Bu$_4$N][PF$_6$]). (----) 0.10 M [n-Bu$_4$N][PF$_6$]. Δf = gold quartz crystal frequency change.

Figure 6 displays the EQCM (i) current and (ii) frequency responses as a function of potential for an Au coated quartz crystal electrode in contact with CH$_3$CN (0.10 M [n-Bu$_4$N][PF$_6$]) in the presence and absence of 0.50 mM of $K^W_{Sn}[N_3C_4H_{10}]$. As shown in Figure 6(ii), the frequency of oscillation of the Au coated quartz crystal remains constant in the absence of $K^W_{Sn}[N_3C_4H_{10}]^{4-}$. In contrast, with 0.50 mM $K^W_{Sn}[N_3C_4H_{10}]^{4-}$ present, and as shown in Figure 6(ii-a) the frequency decreased (mass increased) significantly at potentials more negative than the onset of the $K^W_{Sn}[N_3C_4H_{10}]^{4-/5-}$ process and continued to increase upon reversing the scan direction until reduction of $K^W_{Sn}[N_3C_4H_{10}]^{4-}$ ceased.

Prior to the onset of reduction of $K^W_{Sn}[N_3C_4H_{10}]^{4-}$ minimal frequency (mass) change is detected (Figure 6(ii-b)). Clearly, irreversible surface attachment of a $K^W_{Sn}[N_3C_4H_{10}]^{4-}$ reduction product occurs at a gold electrode and presumably also at GC and Pt electrodes, but to differing extents. This surface modification phenomenon is not present in the modelling, but since it is derived from a $K^W_{Sn}[N_3C_4H_{10}]^{5-}$ reduction product, larger departures in simulated data are expected the more negative the potential or the longer the time since the onset of the $K^W_{Sn}[N_3C_4H_{10}]^{4-/5-}$ process. Use of only the reduction component of data to achieve superior conformance to the simulated data with GC and Au electrodes as implemented in the heuristic form of FTACV data analysis is consistent with this concept.

Spontaneous, electrostatically induced adsorption of POMs often occurs at carbon and metal electrodes [58]. This phenomenon can be detected by so called dipping experiments. Figure S7 shows the results obtained by dipping GC, Au and Pt electrodes in a 0.50 mM solution of $K^W_{Sn}[N_3C_4H_{10}]^{4-}$ for at least 5 minutes, removing the electrodes from the solution, sonicating in CH_3CN, drying and placing the electrode in fresh CH_3CN electrolyte (0.10 M [n-Bu$_4$N][PF$_6$]) solution. No well-defined, surface confined symmetrically shaped, diffusionless voltammetry of adsorbed $K^W_{Sn}[N_3C_4H_{10}]^{4-}$ is evident, as occurs with other POMs [59], nor is there evidence of a grafted POM derivative (see below). However, substantial modification of the background charging current response is evident at Au and Pt electrodes, indicating their electrode surfaces have been modified, but not by attachment of $K^W_{Sn}[N_3C_4H_{10}]^{4-}$.

In order to seek evidence for product interaction with the surface, the electrode potential for a 0.50 mM $K^W_{Sn}[N_3C_4H_{10}]^{4-}$ solution was held at -1.750 V vs Fc$^{0/+}$ for 0, 60, 120, and 180 seconds at the GC, Au and Pt electrodes before commencing cyclic voltammetry. At this potential $K^W_{Sn}[N_3C_4H_{10}]^{4-}$ is reduced to $K^W_{Sn}[N_3C_4H_{10}]^{5-}$ under bulk electrolysis conditions. If surface confined $K^W_{Sn}[N_3C_4H_{10}]^{5-}$ accumulated then stripping current would be expected as occurs in stripping voltammetry [60]. However as shown in Figure 7, no stripping oxidative responses are found at any electrode surface.
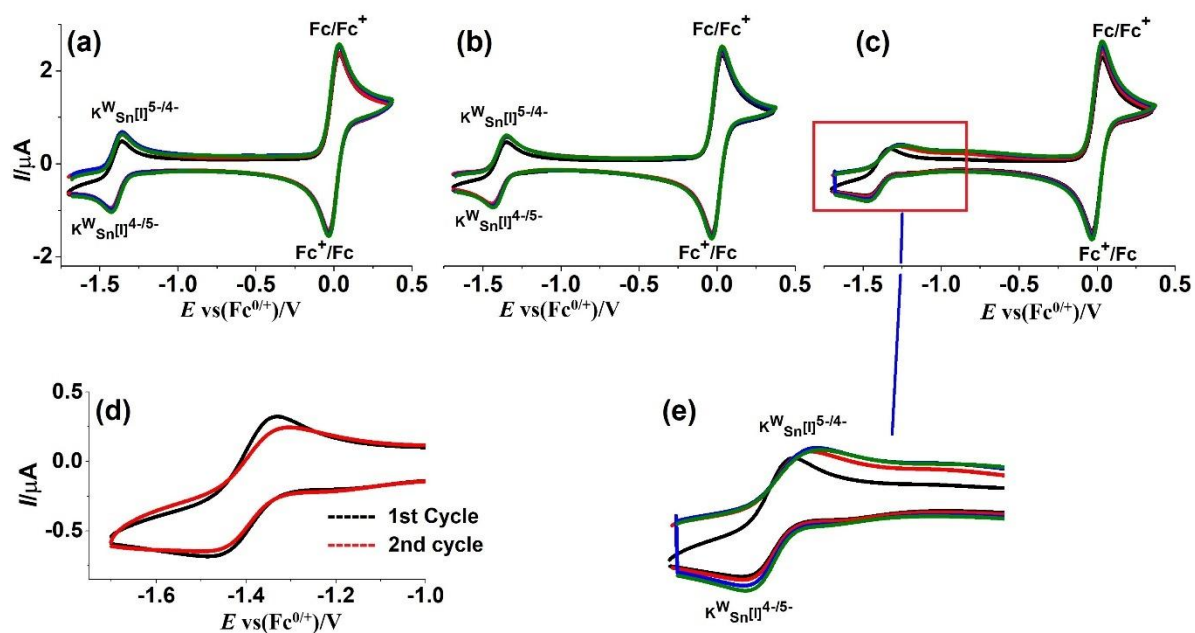
Figure 7. Cyclic voltammetry of 0.50 mM $K^W_{Sn}[N_3C_4H_{10}]^{4-}$ in CH_3CN (0.10 M [n-Bu$_4$N][PF$_6$]) at a scan rate of 0.050 V s^{-1} with (a) GC, (b) Au and (c) Pt electrode ((e) magnified CV of $K^W_{Sn}[N_3C_4H_{10}]^{4-/5-}$ process) when hold the potential at -1.750 V for 0 (**black**), 60 (**red**), 120 (**blue**) and 180 (**green**) s, respectively. (d) first 2 cycles with Pt electrode without hold time.

However, at the Pt electrode (Figure 7 (c) and (e) it is particularly noticeable that the peak-to-peak separation increases with each cycle of potential ($\Delta E_{0\,sec} = 156$ mV, $\Delta E_{60\,sec} = 200$ mV, $\Delta E_{120\,sec} = 219$ mV and $\Delta E_{180\,sec} = 221$ mV), the mid-point potential shifts positively ($E^m_{0\,sec} = -1.408$, $E^m_{60\,sec} = -1.382$, $E^m_{120\,sec} = -1.370$ and $E^m_{180\,sec} = -1.363$ V). Furthermore, the shape of the $K^W_{Sn}[N_3C_4H_{10}]^{4-/5-}$ process changes to a more sigmodal one and the background or charging current increases significantly. The $K^W_{Sn}[N_3C_4H_{10}]^{4-/5-}$ process was less effected in these extended electrolysis experiments at GC and Au electrodes. Cleary, electrode fouling which is most severe with the Pt electrode occurred during the $K^W_{Sn}[N_3C_4H_{10}]^{4-/5-}$ process.

Results of 10 consecutive voltammetric experiments (Figure 8) at each of the GC, Au and Pt electrodes, with no electrode polishing in between each cycle show even more clearly how surface accumulation of a $K^W_{Sn}[N_3C_4H_{10}]^{5-}$ decomposition product gradually facilitates transition from a peak to a sigmodal shaped response. This change in shape is fully analogous to what happens in the

voltammetry of metalloproteins or metalloenzymes upon denaturation [61-63]. Progressive electrode blockage by denatured electroinactive metalloprotein, generates an expanding array of electroactive sites while electrochemistry from residual intact metalloprotein occurs predominantly by radial (sigmoidal shape response) than by linear diffusion (peak shaped response). In the case of the POM used in this study, accumulation of an unknown surface confined product accompanies the initial one-electron reduction, with the impact order being Pt> Au > GC. It is plausible that reduction to $K^W_{Sn}[N_3C_4H_{10}]^{5-}$ lowers the stability of the organic side chain which becomes detached from the POM and provides a pathway for formation of an array of electroinactive sites of unknown composition. Apparently, degradation is more rapid at the Au and Pt electrodes than at GC. Once the electrode is surface modified, the capacitance and other characteristics change progressively with time to give array electrode type behaviour. This nuance implies that the second $K^W_{Sn}[N_3C_4H_{10}]^{5-/6-}$ process at Au and Pt electrodes in particular are far more distorted that the initial $K^W_{Sn}[N_3C_4H_{10}]^{4-/5-}$ process. Thus, accordingly, electrode kinetic FTACV data analysed via the Butler -Volmer model assuming linear diffusion for mass transport should indeed coincide most closely with the modelled data when applied solely to the initial reduction component of the data rather than when using all data that includes the more distorted oxidation component. Effectively, the mass transport model is changing form linear to radial diffusion during the course of the FTACV experiment when fully linear diffusion is assumed throughout in the modelling. However, it should be noted that as expected, repolishing the electrode after 10 experiments restores the voltammetric characteristics shown for the initial one.
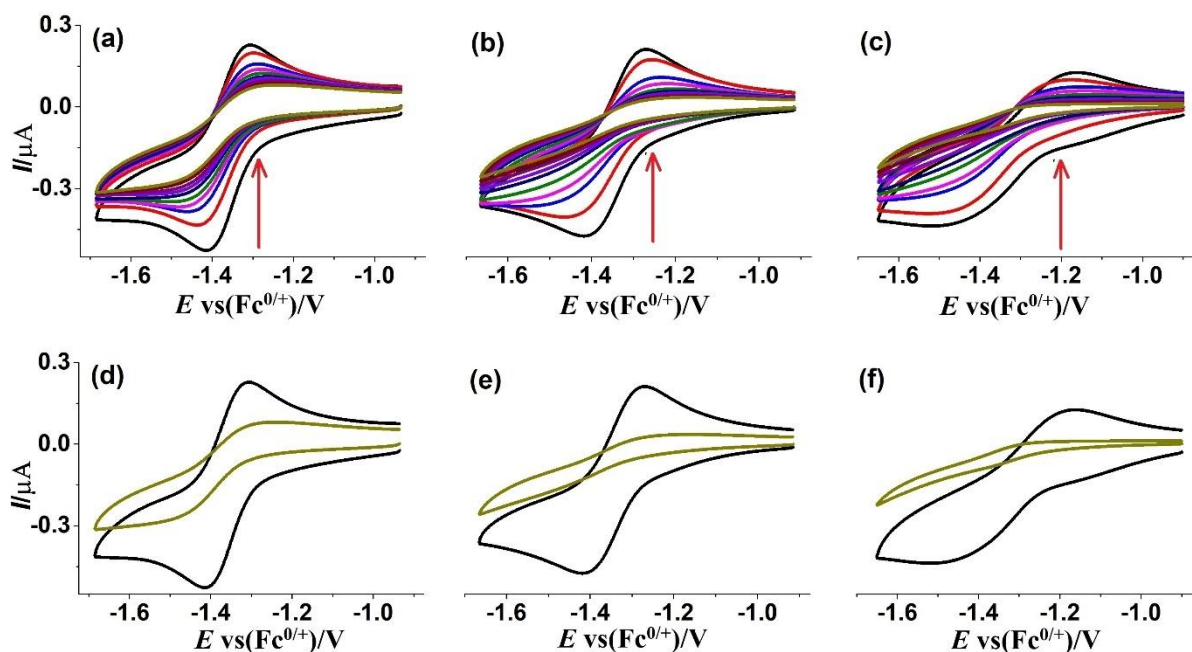
Figure 8.Ten consecutive DC cyclic voltammetric experiments at (a) GC, (b) Au and (c) Pt electrodes without polishing the electrode after each experiment. (d), (e) and (f) represent the 1st and 10th experiments at GC, Au and Pt electrodes, respectively.

3.4 FTACV voltammetric characterization of the grafted $K^W_{Sn}[-]^{4-/5-/6-}$ processes at a GC modified electrode in CH$_3$CN:

Thermodynamic and kinetic parameterisation based on FTAC voltammetry with a sinusoidal perturbation having an amplitude of 80 mV, a frequency of 9.02 Hz and an underlying DC scan rate of (0.052 to 0.086 V s^{-1}) also was applied to FTACV data obtained with the $K^W_{Sn}[-]^{4-}$ modified GC electrode. As in the solution phase exercise described above, more detailed information was expected to emerge than from analysis with the widely used DC voltammetric method [39, 42, 64-67]. The initial simulations used to mimic experimental data for the first reduction process obtained with a $K^W_{Sn}[-]^{4-}$-grafted GC electrode in contact with CH$_3$CN (0.10 M [n-Bu$_4$N][PF$_6$]) solution via heuristic data analysis assumed the values of E^0_{app} = -1.450 V (mid-point potential of DC experiment), with R_u = 518 Ω and Γ = 8.8 × 10^{-11} mol cm^{-2} being known parameters. The outcome of this exercise is shown in Figure 9(i). As for the solution phase studies with $K^W_{Sn}[N_3C_4H_{10}]^{4-}$, simulation-experiment agreement with the second and higher harmonics is good, but background current estimation for the

DC is poor. Values for k_{app}^0 and α_{app} estimated heuristically with this close to monolayer surface coverage were 40 s^{-1} and 0.46 respectively for this first K$^W_{Sn}$[-]$^{4-/5-}$ process. As for the solution soluble scenario described above, estimated k_{app}^0 and α_{app} values are regarded as reliable in the sense that they are derived from simulated data that lie well below that predicted for a reversible process simulated with a very large value of k_{app}^0 and an α_{app} value of 0.50 (Figure 9(ig)).
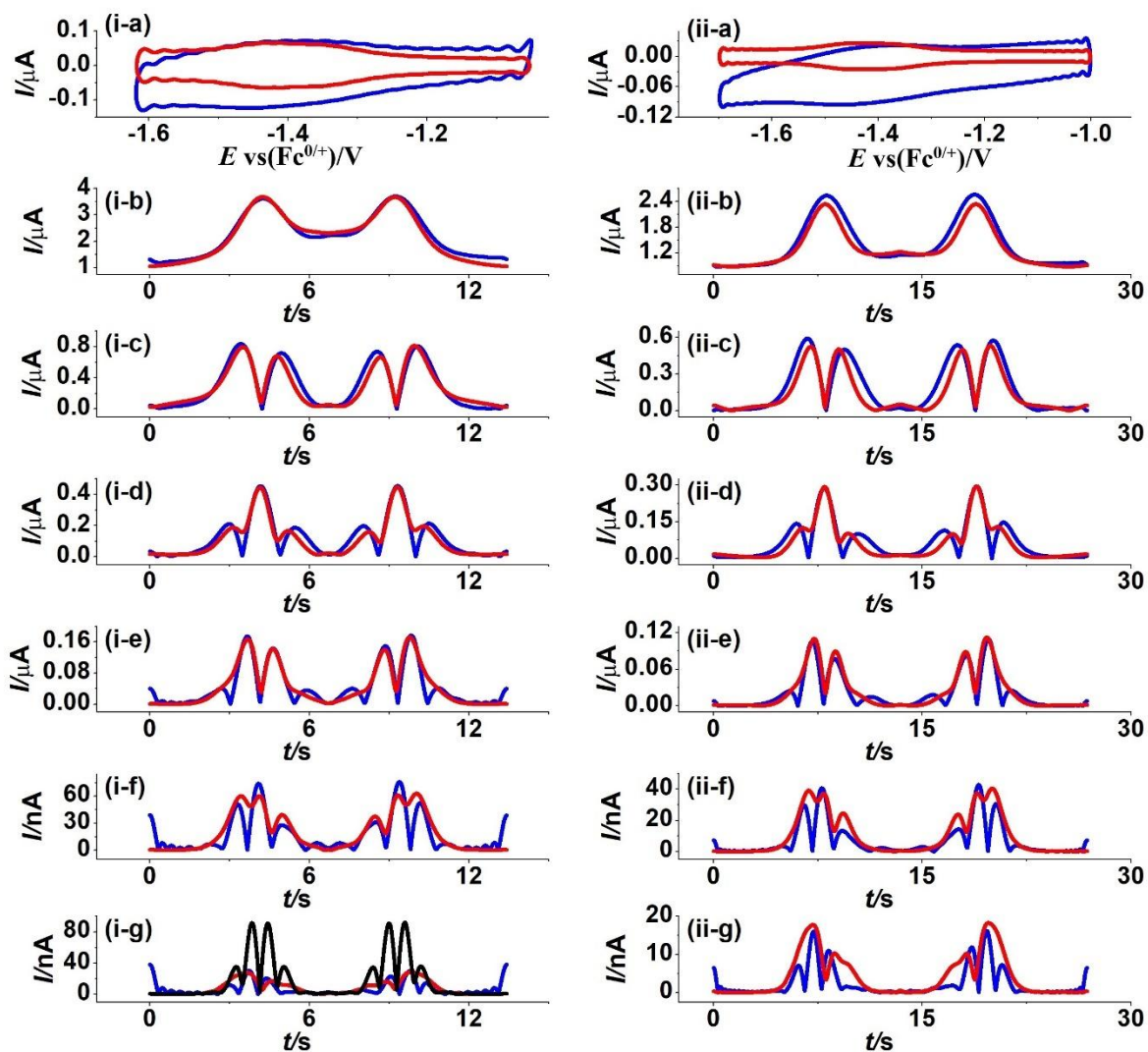
Figure 9. "Best fit" heuristic comparison of simulated (red) and experimental (blue) FTAC voltammetric data obtained for the first reduction process at a K$^W_{Sn}$[-]$^{4-}$-grafted GC electrode in contact with CH$_3$CN (0.10 M [n-Bu$_4$N][PF$_6$]). (i) $\Gamma = 8.8 \times 10^{-11}$ mol cm^{-2} and (ii) $\Gamma = 6.2 \times 10^{-11}$ mol cm^{-2}, $\Delta E = 80$ mV, $f = 9.02$ Hz, $v_i = 0.082$ V s^{-1} and $v_{ii} = 0.052$ V s^{-1}. (a) DC component, (b-g) 1st to 6th harmonic components. Other Parameters used in simulations are given in Table 4. Figure (9 (i-g)) is

comparison of experimental data with that for the sixth harmonic component simulated for a reversible process (black).

The outcome from a second experiment- simulation exercise with a lower, presumably sub-monolayer coverage, ($\Gamma = 6.2 \times 10^{-11}$ mol cm^{-2}) is displayed in Figure 9 (ii) and gave heuristically estimated values of $k_{app}^0 = 38$ s^{-1} and $\alpha_{app} = 0.46$. Again, good theory-experiment agreement was achieved for the second and higher harmonic components that are essentially devoid of background current [66, 68] with relatively poorer agreement for the DC component again attributed to limitations in modelling of the background current for a $K^W_{Sn}[-]^{4-}$-grafted GC electrode. Many POMs [69-73], including those mixed with carbon materials form supercapacitors. Hence, pseudo-capacitance arising from this origin and not accommodated in the model used to mimic the background plausibly is present.

Computer aided data analysis was also applied to parameterise the experimental data for the FTAC voltammetry of $K^W_{Sn}[-]^{4-}$-grafted GC electrode in CH_3CN (0.10 M [n-Bu$_4$N][PF$_6$]). In this data optimisation approach, and as with solution phase studies with $K^W_{Sn}[N_3C_4H_{10}]^{4-}$, E_{app}^0 now was assumed to be an unknown rather than known parameter. Also, electrode kinetic values determined heuristically again were used to select and constrain the parameter space range surveyed. Examination of results of parameterisation by both heuristic and automated methods are summarised in Table 4 and are in excellent agreement.

Table 4. Parameters[a] derived from the heuristic and computer-based comparison of simulated and experimental FTACV data at 9.02 Hz at $K^W_{Sn}[]^{4-}$-grafted GC electrode for the $K^W_{Sn}[]^{4-/5-}$ process in CH_3CN (0.10 M [n-Bu$_4$N][PF$_6$]).

Γ ($\times 10^{-11}$ mol cm^{-2})	Simulation method	R_u (Ω)[b]		E_{app}^0 V vs Fc$^{0/+}$	k_{app}^0 (cm s^{-1})	α_{app}	LS %
8.8 [i]	Heuristic			-1.450	40	0.46	
	Automated	518	Range	-1.455 to -1.446	25 to 50	0.40 to 0.70	
			Estimated	-1.451	41	0.48	82
6.2 [ii]	Heuristic	585		-1.450	38	0.46	
	Automated		Range	-1.455 to -1.446	25 to 45	0.40 to 0.65	

31

| | Estimated | -1.448 | 35 | 0.48 | 84 |

[a] Other parameters used in the simulations are: $A_{GC} = 8.0 \times 10^{-3}$ cm^2, $\Delta E = 80$ mV, $T = 295$ K, $v_i = 0.082$ V s^{-1}, $v_{ii} = 0.052$ V s^{-1} and $f = 9.02$ Hz.

[b] vary due to slight difference in electrode arrangement in cell.

Analysis of both the first and second processes at the $K^W{}_{Sn}[-]^{4-}$-grafted GC electrode simultaneously in one experiment and with $\Gamma = 10 \times 10^{-11}$ mol cm^{-2}, (see Figure 10) gave the results summarized in Table 5. The second process ($k^0_{app2} = 18$ s^{-1}) is kinetically slower than first ($k^0_{app1} = 37$ s^{-1}) according to this analysis of the FTAC voltametric data. This conclusion is consistent with the greater separation in DC cyclic voltammetric peak-to-peak values for the two processes where $\Delta E_{P2} = 37$ mV $> \Delta E_{P1} = 13$ mV (Table 1).
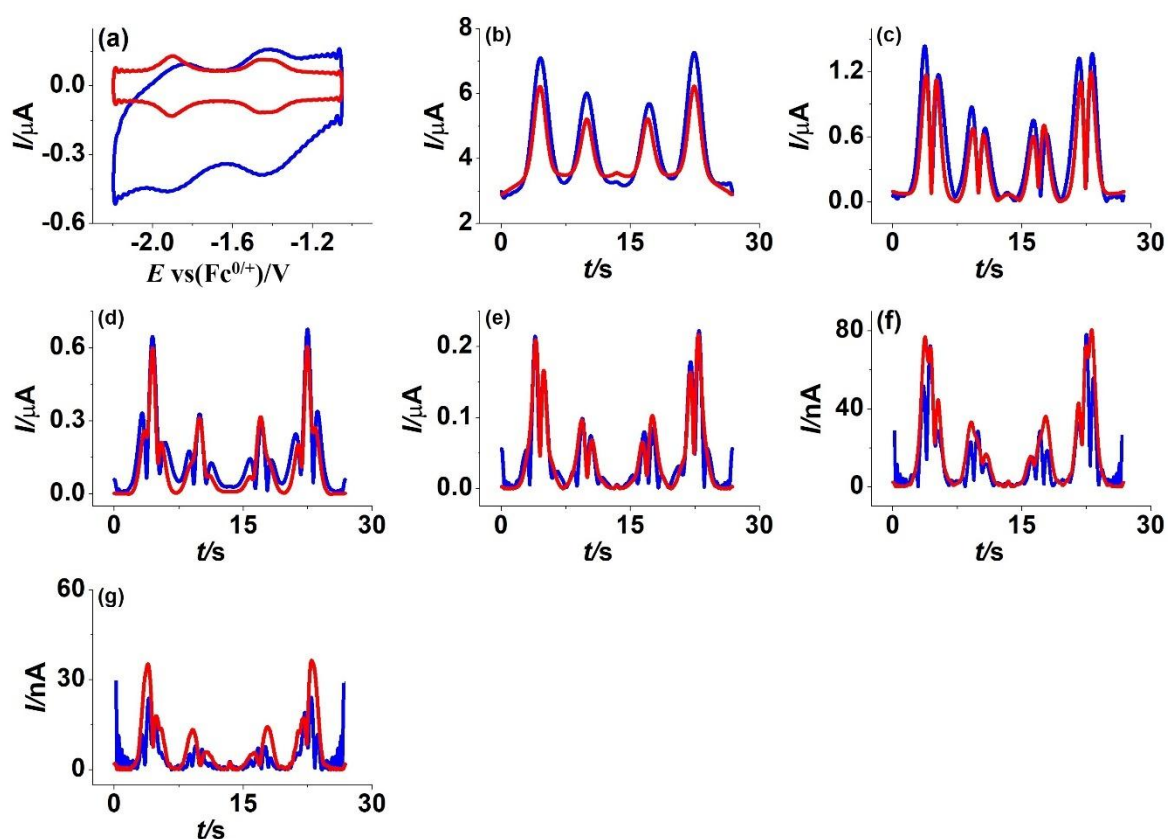
Figure 10. "Best fit" heuristic comparison of simulated (red) and experimental (blue) FTAC voltammetric data for the reduction of a $K^W{}_{Sn}[-]^{4-}$-grafted GC electrode in contact with CH$_3$CN (0.10

M [n-Bu$_4$N][PF$_6$]). Γ = 10 × 10^{-11} mol cm^{-2}, ΔE = 80 mV, f = 9.02 Hz and ν =0.086 V s^{-1}. (a) DC component, (b-g). Other parameters used in simulations are given in Table 5.

Table 5: Parameters[a] derived from the heuristic and computer based comparison of simulated and experimental FTACV data at 9.02 Hz at K$^W_{Sn}$[-]$^{4-}$-grafted (Γ = 10 × 10^{-11} mol cm^{-2}) GC electrode for the K$^W_{Sn}$[-]$^{4-/5-}$ and K$^W_{Sn}$[-]$^{5-/6-}$ processes in CH$_3$CN (0.10 M [n-Bu$_4$N][PF$_6$]).

Simulation method		E^0_{app1}	E^0_{app2}	k^0_{app1}	k^0_{app2}	α_{app1}	α_{app2}	LS %
		V vs Fc$^{0/+}$		cm s^{-1}				
Heuristic		-1.450	-1.920	37	18	0.45	0.46	
Automated	Range	-1.454 to -1.445	-1.924 to -1.914	10 to 60	5 to 35	0.40 to 0.70	0.40 to 0.70	
	Estimated	-1.447	-1.915	40	16	0.48	0.49	77

[a] Other parameters used in the simulations are: A_{GC} = 8.0 × 10^{-3} cm^2, ΔE = 80 mV, T = 295 K, v = 0.086 V s^{-1}, f = 9.02 Hz.

There are again discrepancies between experimental and simulated faradaic current data, this time mainly due non-idealities arising from the presence a highly heterogeneous rather than uniform homogeneous grafted electrode. The cartoon in Figure S8(a) displays all grafted POMs in a fully uniform configuration. However, it is well known that all grafted POM moieties need not be located at the same angle to the flat surface. Furthermore, as in Figure S8(b), grafting of aryl radicals to already grafted arrays leading to multi-layer formation cannot be excluded, nor can interactions with non-grafted POMs. In accordance with probability of non-ideality, it is noted that simulated AC voltammograms have very sharp valleys and peaks with current in between approaching zero. In contrast, in the experimental data the current does not approach close to zero in between these valley and peak features. Rather, the experimental response in all harmonics is more smeared out than in simulated data. This is indicative of thermodynamic and/or kinetic dispersion with a range E^0_{app}, k^0_{app} and α_{app} existing and associated with variability of the distances of the POM redox active framework from the GC surface [45, 74].

In a DC cyclic voltammetric studies of $K^W_{Ge}[-]^{4-}$ and $K^{Mo}_{Sn}[-]^{4-}$ to a GC electrode, Proust and Kanoufi et al [2, 3] used the Laviron method [31] derived from so-called trumpet plots of the reduction and oxidation peak potentials in DC as a function of scan rate to probe the electrode kinetics of these POMs. In their work, considerable departure from theory also was noted , with the goodness of fit to the theory being scan rate dependent. For example, analysis of data in selected scan rate regimes, gave k^0_{app1} values of 800 ($K^W_{Ge}[-]^{4-/5-}$) and 500 s^{-1} ($K^{Mo}_{Sn}[-]^{4-/5-}$). The second process in these studies was even more anomalous having DC cyclic voltammetric peak currents very much smaller than the first process, with a dependence on residual water and adsorption of loosely bound as well as grafted material being reported. Under the very dry conditions used in this study and with heavily sonicated grafted electrodes, the second process for reduction for grafted $K^W_{Sn}[-]^{4-}$ mimics behaviour expected for a quasi-reversible process with k^0_{app} slightly less than about 20 s^{-1} which again is well below the anticipated value for reversible process (Figure 9 (i-g)). In the studies based on DC cyclic voltammetry with related compounds [2, 3], only the experimental peak potential data were compared with theoretical predictions. In this work, slow scan rate data are reported to be independent of potential and hence consistent with a fast reversible process on these relatively long time scales. However, these slow scan rate data are anomalous relative to the model in the context that oxidation and reduction branches are separated by well in excess of 10 mV, which is a characteristic on quasi-reversibility or other non-ideality. In this FTACV study, the entire shape and current magnitudes is considered and evidence for kinetic and/or thermodynamic dispersion is reported.

Modification of theory [75] to accommodate interaction between surface confined redox active moieties sometimes is introduced by employing a Frumkin type isotherm as an alternative to Langmuir one used in this study. In this way interactions between surface confined moieties are modellled. Clearly quantitative studies with surface confined POMs grafted to an electrode are fraught with difficulty. In principle, thermodynamic and kinetic dispersion could have been included in the modelling undertaken in this study along with use of a Frumkin isotherm and indeed are probably

needed. However, this introduces another problem in that containing a unique mathematical solution now becomes daunting with so many extras parameters to be evaluated. Heuristically, the inverse problem would be intractable and data optimisation plagued with lengthy computational times with prospects for numerous localised minima and over- or under parametrisation being high. Thus, we have used the simplest possible model and note that uncertainties are present in reporting electrode kinetic parameter values by either FTACV or DC voltammetric methods. Nevertheless, it is apparent that use of all data rather than just peak potentials is in principle superior in a statistical sense in terms of undertaking experiment-theory comparisons with a pre-selected model. In particular, with grafted moieties present or potentially present from precursors and with substantial POM ion-pairing not included in the model, it is now evident that not only do all the parameters such as E^0_{app}, k^0_{app} and α_{app} estimated as well as the model itself will usually contain unknown levels of uncertainty. Ultimately, sophisticated forms of Bayesian ([76] and references cited therein) or other forms of statistics applied to even more extensive data sets than collected in this FTACV study will be needed to determine which model or models actually provide the best fit to the data; a far from trivial task.

4. Conclusion:

The thermodynamics and electron transfer kinetic parameters associated with the reduction of dissolved $K^W_{Sn}[N_3C_4H_{10}]^{4-}$ at GC, Au and Pt electrodes and the surface confined diazonium derivative $K^W_{Sn}[-]^{4-}$ grafted onto a GC electrode have been derived from FTACV experiments in CH_3CN containing 0.10 M of $[n\text{-}Bu_4N][PF_6]$ as the supporting electrolyte. Both experimenter-based heuristic and computer aided data optimisation approaches have been used to compare experimental and simulated data to provide additional knowledge than could be gleaned by sole use of either method. Discrepancies in experimental and theoretical electrode kinetic data derived using the Butler-Volmer relationship are detected and explained for both dissolved and grafted examples. In solution phase voltammetry, anomalies in the shape of the $K^W_{Sn}[N_3(C_4H_{10})]^{4-/5-}$ process relative to theoretical predictions are evident in the oxidative scan of potential. EQCM experiments at a gold quartz crystal electrode and other experiments at conventional GC, Au and Pt electrodes are indicative of the origin

of the non-ideality being accumulation of an unknown surface confined product that accompanies the initial one-electron reduction, with the order in impact being Pt > Au > GC. Confining data analysis to just the reduction component of the FTACV data set minimises the impact of the introduction of radial diffusion and array like behaviour that are not accommodated in the modelling and establishes that E_{app}^0 values for the $K^W_{Sn}[N_3C_4H_{10}]^{4-/5-}$ process are independent of electrode material as required theoretically and that $k_{appGC}^0 > k_{appAu}^0 > k_{appPt}^0$ with α being close to 0.50 at all electrodes. The same electrode material dependency on k_{app}^0 has been reported for other POMs such as α-$[S_2W_{18}O_{62}]^{4-}$ [48] and $[SVW_{11}O_{40}]^{3-}$ [25]. The impact of accumulated material from decomposition of $K^W_{Sn}[N_3C_4H_{10}]^{5-}$ following the initial elctron transfer step has such a profound effect on the second $K^W_{Sn}[N_3C_4H_{10}]^{5-/6-}$ process that parameterisation of Au and Pt electrode data was not attempted. However at GC, parameterisation remained viable and revealed that k_{app2}^0 for the second process is significantly less than k_{app1}^0 for the first. This same order, $k_{app1}^0 > k_{app2}^0$, also applies to reduction of grafted $K^W_{Sn}[-]^{4-}$. However, discrepancies in experimental and simulated FTACV data with this surface confined POM are attributed predominantly to the presence of thermodynamic and kinetic dispersion arising from heterogeneity in the grafted GC surface. The relatively sluggish electrode kinetics encountered in the dynamic electrochemistry of $K^W_{Sn}[N_3C_4H_{10}]^{4-}$ may be due to the long organic chain hindering the approach of the POM to the electrode surface, although differences in ion-paring and other factors also may play a role.

As might be anticipated, E^0 values for both solution soluble $K^W_{Sn}[N_3C_4H_{10}]^{4-}$ and the surface confined $K^W_{Sn}[-]^{4-}$ derivative are similar. The thermodynamics for the POMs are mostly controlled by the transition metal in the core framework. Thus, very similar E_{app}^0 values are found when either Sn or Ge side chains are attached to W based frameworks while much less negative E_{app}^0 values are found with Mo-functionalized POMs.

References:

1.   Kuhn, A., N. Mano, and C. Vidal, *Polyoxometalate modified electrodes: from a monolayer to multilayer structures.* Journal of Electroanalytical Chemistry, 1999. **462**(2): p. 187-194.

2.   Rinfray, C., et al., *Electron Transfer to a Phosphomolybdate Monolayer on Glassy Carbon: Ambivalent Effect of Protonation.* Inorganic Chemistry, 2016. **55**(14): p. 6929-6937.

3.   Rinfray, C., et al., *Electrografting of diazonium-functionalized polyoxometalates: synthesis, immobilisation and electron-transfer characterisation from glassy carbon.* Chemistry, 2013. **19**(41): p. 13838-46.

4.   Sadakane, M. and E. Steckhan, *Electrochemical Properties of Polyoxometalates as Electrocatalysts.* Chemical Reviews, 1998. **98**(1): p. 219-238.

5.   Han, Z., et al., *Inorganic–organic hybrid polyoxometalate containing supramolecular helical chains: Preparation, characterization and application in chemically bulk-modified electrode.* Electrochimica Acta, 2005. **51**(2): p. 218-224.

6.   Song, W., et al., *Application of the sol-gel technique to polyoxometalates: towards a new chemically modified electrode.* Electrochimica Acta, 2000. **45**(10): p. 1639-1644.

7.   Toma, F.M., et al., *Efficient water oxidation at carbon nanotube–polyoxometalate electrocatalytic interfaces.* Nature Chemistry, 2010. **2**(10): p. 826.

8.   Bonastre, J., et al., *Electrochemical and chemical characterization of polypyrrole/phosphotungstate coatings electrosynthesized on carbon steel electrodes in acetonitrile medium.* Synthetic Metals, 2009. **159**(17-18): p. 1723-1730.

9.   Liu, S., et al., *Fast and sensitive colorimetric detection of H2O2 and glucose: a strategy based on polyoxometalate clusters.* ChemPlusChem, 2012. **77**(7): p. 541-544.

10.   Mercier, D., et al., *Polyoxometalate nanostructured gold surfaces for sensitive biosensing of benzo [a] pyrene.* Sensors and Actuators B: Chemical, 2015. **209**: p. 770-774.

11.   Chen, J.-J., M.D. Symes, and L. Cronin, *Highly reduced and protonated aqueous solutions of [P 2 W 18 O 62] 6– for on-demand hydrogen generation and energy storage.* Nature chemistry, 2018. **10**(10): p. 1042-1047.

12.   Nishimoto, Y., et al., *Super-reduced polyoxometalates: excellent molecular cluster battery components and semipermeable molecular capacitors.* Journal of the American Chemical Society, 2014. **136**(25): p. 9042-9052.

13.   Kinoshita, K., *Carbon: electrochemical and physicochemical properties.* 1988.

14.   McCreery, R.L., *Carbon electrodes: structural effects on electron transfer kinetics.* Electroanalytical chemistry, 1991. **17**: p. 221-374.

15.   Zhang, W., et al., *Recent development of carbon electrode materials and their bioanalytical and environmental applications.* Chemical Society Reviews, 2016. **45**(3): p. 715-752.

16.   Liu, H., et al., *An ionic liquid-type carbon paste electrode and its polyoxometalate-modified properties.* Electrochemistry Communications, 2005. **7**(12): p. 1357-1363.

17.   Zhou, M., et al., *Electrochemistry and electrocatalysis of polyoxometalate-ordered mesoporous carbon modified electrode.* Analytica Chimica Acta, 2007. **587**(1): p. 124-131.

18.   Sung, H., H. So, and W.-k. Paik, *Polypyrrole doped with heteropolytungstate anions.* Electrochimica Acta, 1994. **39**(5): p. 645-650.

19.   Cheng, L. and J.A. Cox, *Nanocomposite Multilayer Film of a Ruthenium Metallodendrimer and a Dawson-Type Polyoxometalate as a Bifunctional Electrocatalyst.* Chemistry of Materials, 2002. **14**(1): p. 6-8.

20.   Martel, D. and A. Kuhn, *Electrocatalytic reduction of H2O2 at P2Mo18O626– modified glassy carbon.* Vol. 45. 2000. 1829-1836.

21.   Proust, A., et al., *Functionalization and post-functionalization: a step towards polyoxometalate-based materials.* Chemical Society Reviews, 2012. **41**(22): p. 7605-7622.

22.   Volatron, F., et al., *Electron transfer properties of a monolayer of hybrid polyoxometalates on silicon.* Journal of Materials Chemistry C, 2015. **3**(24): p. 6266-6275.

23.   Li, J., et al., *Influence of 1-butyl-3-methylimidazolium on the electron transfer kinetics associated with the [SVW11O40] 3–/4–(VV/IV) and [SVW11O40] 4–/5–(WVI/V) processes in dimethylformamide.* Journal of Electroanalytical Chemistry, 2016. **779**: p. 67-74.

24.   Li, J., A.M. Bond, and J. Zhang, *Probing electrolyte cation effects on the electron transfer kinetics of the [α-SiW12O40] 4–/5– and [α-SiW12O40] 5–/6– processes using a boron-doped diamond electrode.* Electrochimica Acta, 2015. **178**: p. 631-637.

25.   Li, J., et al., *Electrode material dependence of the electron transfer kinetics associated with the [SVW11O40] 3–/4–(VV/IV) and [SVW11O40] 4–/5–(WVI/V) processes in dimethylformamide.* Electrochimica Acta, 2016. **201**: p. 45-56.

26.   Choi, S.-H. and J.-W. Kim, *Adsorption properties of Keggin-type polyoxometalates on carbon based electrode surfaces and their electrocatalytic activities.* Bulletin of the Korean Chemical Society, 2009. **30**(4): p. 810-816.

27.   Fleming, B.D. and A.M. Bond, *DC and AC voltammetry of a free-base porphyrin adsorbed onto basal-plane graphite under acidic conditions: An example of a close to ideal reversible two-electron surface-confined redox process at sub-monolayer coverages.* Electrochimica Acta, 2009. **54**(10): p. 2713-2719.

28.   Guziejewski, D., V. Mirceski, and D. Jadresko, *Measuring the electrode kinetics of surface confined electrode reactions at a constant scan rate.* Electroanalysis, 2015. **27**(1): p. 67-73.

29.   Huder, L., et al., *Evidence for charge transfer at the interface between hybrid phosphomolybdate and epitaxial graphene.* Langmuir, 2016. **32**(19): p. 4774-4783.

30.   Laviron, E., L. Roullier, and C. Degrand, *A multilayer model for the study of space distributed redox modified electrodes: Part II. Theory and application of linear potential sweep voltammetry for a simple reaction.* Journal of Electroanalytical Chemistry and Interfacial Electrochemistry, 1980. **112**(1): p. 11-23.

31.   Laviron, E., *General expression of the linear potential sweep voltammogram in the case of diffusionless electrochemical systems.* Journal of Electroanalytical Chemistry and Interfacial Electrochemistry, 1979. **101**(1): p. 19-28.

32.   Kennedy, G.F., *MECSim software package*. 2018.

33.   Kennedy, G.F., A.M. Bond, and A.N. Simonov, *Modelling ac voltammetry with MECSim: facilitating simulation–experiment comparisons.* Current Opinion in Electrochemistry, 2017. **1**(1): p. 140-147.

34.   Morris, G.P., et al., *A comparison of fully automated methods of data analysis and computer assisted heuristic methods in an electrode kinetic study of the pathologically variable [Fe (CN) 6] 3–/4–process by AC voltammetry.* Analytical chemistry, 2013. **85**(24): p. 11780-11787.

35.   Laurans, M., et al., *Molecular signature of polyoxometalates in electron transport of silicon-based molecular junctions.* Nanoscale, 2018. **10**(36): p. 17156-17165.

36.   Sawyer, D., A. Sobkowiak, and J. Roberts Jr, *Electrochemistry for Chemists, ; John Wiley&Sons*. Inc.: New York. 1995.

37.   Bond, A.M., et al., *Changing the look of voltammetry*. 2005, ACS Publications.

38.   Bard, A.a.F., Larry R, *Electrochemical Methods: Fundamentals and applications*. 2nd ed. 2001, New York: Wiley.

39.   Zhang, J., S.-X. Guo, and A.M. Bond, *Discrimination and evaluation of the effects of uncompensated resistance and slow electrode kinetics from the higher harmonic components of a Fourier transformed large-amplitude alternating current voltammogram.* Analytical Chemistry, 2007. **79**(6): p. 2276-2288.

40.   Gritzner, G. and J. Kuta, *Recommendations on reporting electrode potentials in nonaqueous solvents (Recommendations 1983).* Pure and applied chemistry, 1984. **56**(4): p. 461-466.

41.   Rudolph, M., D.P. Reddy, and S.W. Feldberg, *A simulator for cyclic voltammetric responses.* Analytical chemistry, 1994. **66**(10): p. 589A-600A.

42.   Guo, S., et al., *Fourier transform large-amplitude alternating current cyclic voltammetry of surface-bound azurin.* Analytical Chemistry, 2004. **76**(1): p. 166-177.

43. Zhang, J., et al., *Novel kinetic and background current selectivity in the even harmonic components of Fourier transformed square-wave voltammograms of surface-confined azurin.* The Journal of Physical Chemistry B, 2005. **109**(18): p. 8935-8947.

44. Fourmond, V. and C. Léger, *Modelling the voltammetry of adsorbed enzymes and molecular catalysts.* Current Opinion in Electrochemistry, 2017. **1**(1): p. 110-120.

45. Morris, G.P., et al., *Theoretical analysis of the relative significance of thermodynamic and kinetic dispersion in the dc and ac voltammetry of surface-confined molecules.* Langmuir, 2015. **31**(17): p. 4996-5004.

46. Bond, A.M., et al., *Characterization of nonlinear background components in voltammetry by use of large amplitude periodic perturbations and Fourier transform analysis.* Analytical chemistry, 2009. **81**(21): p. 8801-8808.

47. Li, J., et al., *Impact of sp2 Carbon Edge Effects on the Electron Transfer Kinetics of the Ferrocene/Ferricenium Process at a Boron Doped Diamond Electrode in an Ionic Liquid.* The Journal of Physical Chemistry C, 2019.

48. Rahman, M.A., et al., *Modelling limitations encountered in the thermodynamic and electrode kinetic parameterization of the α-[S2W18O62] 4−/5−/6− processes at glassy carbon and metal electrodes.* Journal of Electroanalytical Chemistry, 2019: p. 113786.

49. Bard, A., R. Parsons, and J. Jordan, *Standard Potentials in Aqueous Solution 1985.* M. Dekker.

50. Laviron, E., *Adsorption, autoinhibition and autocatalysis in polarography and in linear potential sweep voltammetry.* Journal of Electroanalytical Chemistry and Interfacial Electrochemistry, 1974. **52**(3): p. 355-393.

51. Poblet, J.M., X. López, and C. Bo, *Ab initio and DFT modelling of complex materials: towards the understanding of electronic and magnetic properties of polyoxometalates.* Chemical Society Reviews, 2003. **32**(5): p. 297-308.

52. Hinrichs, K., et al., *Analytical methods for the characterization of aryl layers*. 2012: Wiley-VCH Verlag GmbH & Co. KGaA: Weinheim.

53. Nicholson, R.S., *Theory and application of cyclic voltammetry for measurement of electrode reaction kinetics.* Analytical chemistry, 1965. **37**(11): p. 1351-1355.

54. Sauerbrey, G., *The use of quarts oscillators for weighing thin layers and for microweighing.* Z. Phys., 1959. **155**: p. 206-222.

55. Gooding, J.J., *Advances in interfacial design for electrochemical biosensors and sensors: aryl diazonium salts for modifying carbon and metal electrodes.* Electroanalysis: An International Journal Devoted to Fundamental and Practical Aspects of Electroanalysis, 2008. **20**(6): p. 573-582.

56. Liu, G., T. Böcking, and J.J. Gooding, *Diazonium salts: Stable monolayers on gold electrodes for sensing applications.* Journal of Electroanalytical Chemistry, 2007. **600**(2): p. 335-344.

57. Liu, G., et al., *A comparative study of the modification of gold and glassy carbon surfaces with mixed layers of in situ generated aryl diazonium compounds.* Electroanalysis: An International Journal Devoted to Fundamental and Practical Aspects of Electroanalysis, 2010. **22**(9): p. 918-926.

58. Liu, S., et al., *Electrochemical preparation and characterization of silicotungstic heteropolyanion monolayer electrostatically linked aminophenyl on carbon electrode surface.* Langmuir, 1999. **15**(21): p. 7268-7275.

59. Robinson, M., et al., *Models and their limitations in the voltammetric parameterisation of the six electron surface confined reduction of [PMo12O40] 3-at glassy carbon and boron doped diamond electrodes.* ChemElectroChem, 2019.

60. Choi, S.M., et al., *Effect of polyoxometalate amount deposited on Pt/C electrocatalysts for CO tolerant electrooxidation of H2 in polymer electrolyte fuel cells.* international journal of hydrogen energy, 2010. **35**(13): p. 6853-6862.

61. Bogdanovskaya, V., et al., *Electrochemical transformations of proteins adsorbed at carbon electrodes.* Bioelectrochemistry and Bioenergetics, 1988. **19**(3): p. 581-584.

62. Pletcher, D., et al., *Instrumental methods in electrochemistry*. 2001: Elsevier.

63. Salvatore, P., et al., *Electrochemistry of Single Metalloprotein and DNA-Based Molecules at Au (111) Electrode Surfaces.* ChemPhysChem, 2013. **14**(10): p. 2101-2111.

64. Fleming, B.D., et al., *Separation of electron-transfer and coupled chemical reaction components of biocatalytic processes using Fourier transform ac voltammetry.* Analytical chemistry, 2005. **77**(11): p. 3502-3510.

65. Fleming, B.D., et al., *Detailed analysis of the electron-transfer properties of azurin adsorbed on graphite electrodes using dc and large-amplitude Fourier transformed ac voltammetry.* Analytical chemistry, 2007. **79**(17): p. 6515-6526.

66. O'Mullane, A.P., et al., *Higher harmonic large-amplitude fourier transformed alternating current voltammetry: analytical attributes derived from studies of the oxidation of ferrocenemethanol and uric acid at a glassy carbon electrode.* Analytical chemistry, 2008. **80**(12): p. 4614-4626.

67. Sher, A.A., et al., *Resistance, capacitance, and electrode kinetic effects in fourier-transformed large-amplitude sinusoidal voltammetry: Emergence of powerful and intuitively obvious tools for recognition of patterns of behavior.* Analytical chemistry, 2004. **76**(21): p. 6214-6228.

68. Zhang, J., et al., *Large-amplitude Fourier transformed high-harmonic alternating current cyclic voltammetry: kinetic discrimination of interfering faradaic processes at glassy carbon and at boron-doped diamond electrodes.* Analytical chemistry, 2004. **76**(13): p. 3619-3629.

69. Brousse, T., et al., *Capacitive and pseudocapacitive electrodes for electrochemical capacitors and hybrid devices*, in *Metal Oxides in Supercapacitors*. 2017, Elsevier. p. 1-24.

70. Dubal, D.P., P. Gómez-Romero, and G. Korotcenkov, *Metal oxides in supercapacitors*. 2017: Elsevier.

71. Genovese, M. and K. Lian, *Polyoxometalate modified inorganic–organic nanocomposite materials for energy storage applications: A review.* Current Opinion in Solid State and Materials Science, 2015. **19**(2): p. 126-137.

72. Hu, C., et al., *Aqueous solutions of acidic ionic liquids for enhanced stability of polyoxometalate-carbon supercapacitor electrodes.* Journal of Power Sources, 2016. **326**: p. 569-574.

73. Ruiz, V., J. Suárez-Guevara, and P. Gomez-Romero, *Hybrid electrodes based on polyoxometalate–carbon materials for electrochemical supercapacitors.* Electrochemistry Communications, 2012. **24**: p. 35-38.

74. Rowe, G.K., et al., *Consequences of kinetic dispersion on the electrochemistry of an adsorbed redox-active monolayer.* Langmuir, 1995. **11**(5): p. 1797-1806.

75. Laviron, E. and L. Roullier, *General expression of the linear potential sweep voltammogram for a surface redox reaction with interactions between the adsorbed molecules: applications to modified electrodes.* Journal of Electroanalytical Chemistry and Interfacial Electrochemistry, 1980. **115**(1): p. 65-74.

76. Lambert, B., *A student's guide to Bayesian statistics*. 2018: Sage.